WILEY-VCH

DOI: 10.1002/ ((please add manuscript number))
Article type: Review

Recent advance in improving the stability of perovskite solar cells

Nguyen Huy Tiep[#], Zhiliang Ku[#], Hong Jin Fan[*]

N.H. Tiep, Dr. Z. L. Ku, Prof. H. J. Fan

School of Physical and Mathematical Sciences, Nanyang Technological University, Singapore 637371, Singapore

Email: fanhj@ntu.edu.sg

N.H. Tiep

Energy Research Institute @ NTU, Interdisciplinary Graduate School, Nanyang Technological University, Singapore 637553, Singapore

N.H. Tiep and Z. L. Ku contributed equally to this work.

KEYWORDS: perovskite solar cells; air stability; organic-inorganic lead halide

Abstract

Organometal trihalide perovskite have recently emerged as promising materials for low-cost, high-efficiency solar cells. In less than five years, the efficiency of perovskite solar cells (PSC) has been updated rapidly as a result of new strategies that are adopted in its fabrication process, including device structure, interfacial engineering, chemical compositional tuning, and the crystallization kinetics control. Up to now, the champion efficiency of PSC has reached 20.1%, which is close to that of single crystal silicon solar cells. However, the stability of PSC devices is still unsatisfactory and becomes the main bottleneck that impedes their commercialization. Here, we summarize the recent study on the degradation mechanisms of organometal trihalide perovskites in PSC devices and the strategies for stability improvement.

Introduction

Solar energy has been considered as the most promising new energy resource due to its advantages of cleanness, sustainability, and safety. Photovoltaic devices work based on the simple photoelectric effect, that photons falling on a semiconductor can create electron–hole pairs, which can be separated by an electric potential difference across the interface of two different materials, forming electricity.[1, 2] Several kinds of solar cells have been invented in the past decades and they are overall divided into three generations.[3] The first generation solar cell refers to a single p-n junction of crystalline silicon, exhibiting high power conversion efficiency (PCE) up to 25.6% (Panasonic, Japan). The second generation, typically based on cadmium telluride (CdTe) or copper indium gallium selenide/sulfide (CIGS), demonstrate so far champion PCE of 21.7% (ZSW, Germany).[4] So far, commercial photovoltaic market has been dominated by the first two generation solar cells because of their high PCE and excellent stability. However, they also suffer from relatively high production cost at large scale due to tedious and complicate processing condition, which may escalates their payback time. This calls for the development of new types of cost effective, easy processable solar cells with high efficiency.

The third generation solar cells, including dye-sensitized solar cells (DSSCs)[5, 6] and organic photovoltaics (OPV)[7, 8], have gained substantial attraction since its emergence at end of last century. In contrast to the high cost purification process or vacuum deposition method required for the first two generation solar cells, DSSCs and OPV can be fabricated by facile printing technique such as screen-printing, doctor blading, and spin-coating. This cost effectiveness is considered as one of the most significant attractive characteristic. After decades of effort, scientists have developed the PCE of DSSCs and OPV up to 13% and 10.6%, respectively.[9, 10] Judging only by the PCE, it seems that the photovoltaic market will continue be dominated by the first two generation solar cells. However, this dominance is now being challenged by the emergence of a new light absorber based on organic-metal halide perovskite (such as $CH_3NH_3PbI_3$).

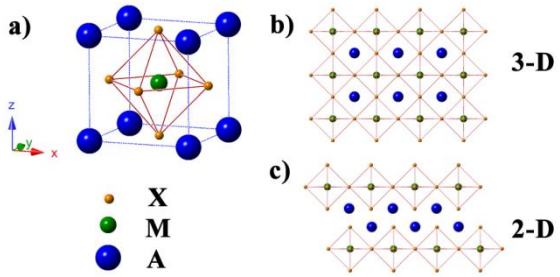

Fig. 1 a) Crystal structure of organometal perovskite AMX_3 with cubic symmetry. b) Projected view of the 3D perovskite (AMX_3) and c) the 2D layered perovskite (A_2MX_4).

Generally speaking, compounds that have the same crystal structure as $CaTiO_3$ are known as perovskites. The conventional perovskites can be overall classified into inorganic oxide perovskites, alkali halide perovskites, and organic-metal halide perovskites. All can be represented by simple building block AMX_3, where M is metal cation and X an anion consisting of oxide or halide (see Fig. 1a). The M and X ions form a MX_6 octahedral geometry with M at the center and X at the corners. By connecting through the corners, the MX_6 octahedral extends to form a three dimensional structure (see Fig. 1b). In case of organic-metal halide perovskite, the A cation represents organic cation and fills the cuboctahedral holes. The prerequisite for a closed-packed perovskite structure is that the size of the A cation must fit these cuboctahedral holes. In an idea perovskite with a cubic space group Pm3m, the ions in the compound are considered to be perfectly packed and their ionic radii have the geometrical relationship of $r_A + r_X = \sqrt{2}\,(r_M + r_X)$, where r_A, r_M and r_X are the ionic radii of A, M and X, respectively.[11] It is known that Goldschmidt proposed a tolerance factor t to describe the structural non-perfection in early 1920s,[12] which can be described as: $t = (r_A + r_X)/\sqrt{2}(r_M + r_X)$. For the whole perovskite-type materials, t is in the range of approximately $0.78 < t < 1.05$, although there is a slight expanded range for distorted structures. It should be noted that the tolerance factor is calculated based on the ionic radius and ought to be only used as an estimation because perovskite are not exclusively ionic. Generally, in organic-metal halide perovskite, A cation consists of three or less C–C or C–N bonds. The most common examples are methylammonium ($CH_3NH_3^+$, MA),[13] ethylammonium ($CH_3CH_2NH_3^+$, EA),[14] tetramethylammonium ($N(CH_3)_4^+$, TMA)[15, 16] and formamidinium ($NH_2CHNH_2^+$, FA)[17, 18] etc. With different ions, the perovskite materials actually have pseudo-cubic or distorted cubic structure. Any distortion will affect physical properties of perovskite materials, such as electronic, optical, magnetic and dielectric

properties. Furthermore, layered perovskites with two-dimensional (2-D) structure are formed by alternating the organic and inorganic in the structure. As shown in Fig. 1c, the simplest layered perovskite consists of MX_4^{2-} layers of corner-sharing metal halide octahedral, yielding the general formula of A_2MX_4. Note that, in contrast to the 3-D perovskites, layered perovskites with 2-D structure can accommodate much larger and more complex organic cations, since the cage into which the organic cation must fit is no longer confined in three dimensions.[19] Most importantly, different organic cations substituted into a perovskite family could have a drastic impact on the chemical and physical properties.[20-22]

Methylammonium-metal halide perovskites with the general formula of $CH_3NH_3MX_3$ where X=Sn, Pb and X=Cl, Br, I have been widely reported.[23-28] Due to their high charge carrier mobility, they have been successfully utilized as an active layer in field effect transistors and electroluminescent devices before entering the domain of solar cells.[29-34] In addition, the band gap value can be tailored through changing the alkyl group, or metal atom and halide.[35-38] The tunable optical and electronic properties, together with the large absorption coefficient[35] and high charge carrier mobility and long diffusion length,[32] make perovskites a promising material in photovoltaic.

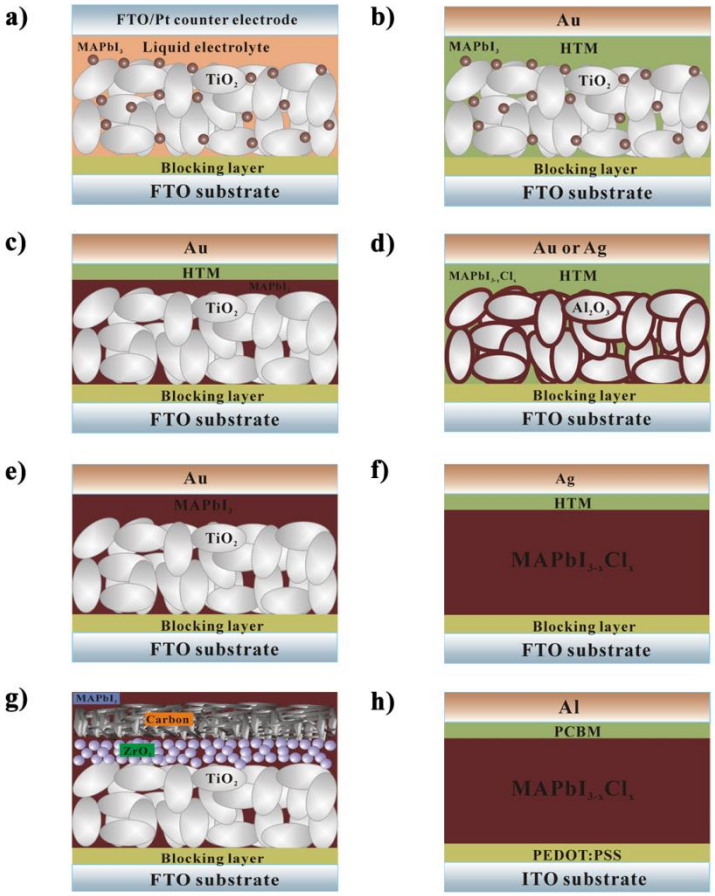

Fig. 2 Different structures of perovskite-based solar cells: a) Liquid-state perovskite-sensitized solar cell, b) Solid-state perovskite-sensitized solar cell, c) Mesoscopic solar cell, d) Meso-superstructured solar cell, e) Mesoscopic heterojunction solar cell, f) Planar heterojunction solar cell, g) Fully printable mesoscopic heterojunction solar cell, h) Invert planar heterojunction solar cell.

In 2009, Miyasaka and co-workers firstly utilized $MAPbI_3$ and $MAPbBr_3$ perovskite nanocrystal as light absorber in liquid electrolyte-based DSSCs.[39] This perovskite solar cell (PSC) followed the structure of DSSCs, which employ mesoporous nanocrystalline TiO_2 as the host of light absorber and iodide/triiodide-based redox as electrolyte (Fig. 2a). Although the PCEs were moderate (3.8% for the $MAPbI_3$, 3.13% for the $MAPbBr_3$) and the stability was poor in liquid electrolyte configuration, this PSC actually has opened up a new path for another kind of new generation solar cell with high efficiency. Subsequently in 2011, Park and co-workers bumped up the PCE of $MAPbI_3$ cell to 6.54%, while the same device based on N719 dye showed much lower PCE (3.89%).[40] However, this PCE was still unsatisfactory and requires further enhancement. The breakthrough of PSC came in 2012, when several groups took the lead in reporting that the solid-state hole-transporting material (HTM) Spiro-OMETAD[41] could perform as an effective electrolyte for PSC.[42, 43] Grätzel teamed up with Park fabricated PSC with a structure evolving from solid-state DSSCs (Fig. 2b) and reported a remarkable PCE of 9.7%.[44] Nearly at the same time, Snaith in collaboration with Miyasaka discovered that the n-type TiO_2 can be replace by an insulator, Al_2O_3, acting as a scaffold in a device coined as "meso-superstructured" PSC (Fig. 2d).[43] The combination of a mixed halide perovskite ($MAPbI_{3-x}Cl_x$) as light harvester on top of the Al_2O_3 film gave a record PCE of 10.9%.[43] The authors claimed that compared with the n-type TiO_2 film, insulating Al_2O_3 scaffold avoids the voltage drop associated with the occupation of the TiO_2 band-tails and generates a high open circuit voltage (V_{oc}) of 1.13 V. This result established that the perovskite material can function as both light absorber and electron transport material. Soon after that, it was also demonstrated that, interestingly, perovskite can act both as an efficient light absorber and a p-type hole-transporter in $MAPbI_3/TiO_2$ heterojunction PSC (see Fig. 2e).[45] The combination of different perovskites, as n-type and as p-type, may pave a new path towards another new kind of solar cells.

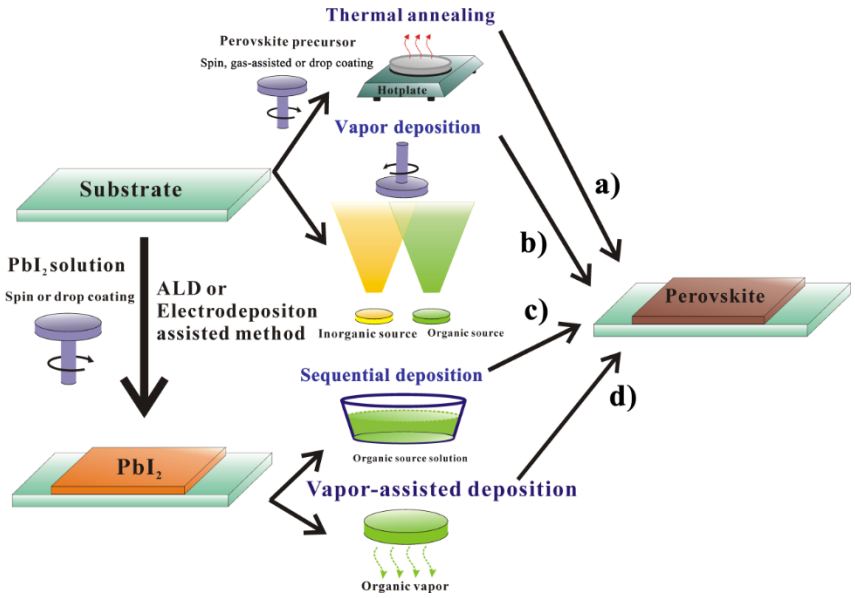

Fig. 3 Different methods for preparing perovskite: a) "One-step" method, including gas-assisted spin coating, drop coating, ultrasonic spray-coating and doctor-blading; b) Vapor deposition method; c) Sequential deposition method, including ALD-assisted method and electrodeposition assisted method, d) Vapor-assisted solution method.

Since the middle of 2013, several innovations of the cell fabrication technique were reported, and high PCEs (>12%) were achieved by using these new methods (see summary in Fig. 3). First was the sequential deposition method, including ALD[49] and electrodeposition assisted method[50] for the deposition of PbI_2 (see Fig. 3c). The eventual perovskite on mesoporous TiO_2 led to a PCE of 15% and a certified value of 14.1% with high reproducibility.[52, 53] Then the vapor deposition (see Fig.3b) method gives a PCE of 15.4% in the planar heterojunction PSC (see Fig. 2f).[54] Similar vacuum deposition method was used for the preparation of uniform perovskite films in another planar-type PSC, with the structure evolved from organic photovoltaics (see Fig. 2h).[55] After that, the vapor-assisted solution process (see Fig. 3d) also provided a simple approach to perovskite film preparation, and the planar heterojunction PSC fabricated by this method showed a PCE of 12.1%.[51] Very recently, the Han group reported a carbon-based full-printable PSC (see Fig. 2g)[56] with a certified PCE of 12.8% and ambient stability over 1000 h under solar irradiation.[57] In this printable PSC, the most simplest and scalable "one-step method" (Fig. 3a) was employed for the deposition of perovskite. Moreover, some other "one step" techniques, such as gas-assisted spin coating,[46] ultrasonic spray-coating[47] and doctor-blading,[48] have been also utilized to obtain promising performance on PSC.

Up to now, the record PCE is 20.1%[58] held by the researchers from Korean Research Institute of Chemical Technology, and the Yang group in UCLA has reported a PCE up to 19.3% in a planar geometry.[59] In comparison to the PCE of the first two generation solar cells (25% for crystalline Silicon solar cell and 21.7% for CIGS solar cell), these third generation PSCs have exhibited great potential for commercial application due to their apparent tolerance of defects, extremely low cost and ease of fabrication.[60] *However*, the PSCs that top two in the NREL efficiency chart are labeled with the feature of "not stabilized".[61] In recent years, researchers have made great efforts in pursuing high PCE values but generally neglected the stability issue of PSCs. As summarized by Wang and co-workers,[62] perovskite materials suffered from several kinds of stability problems in PSCs. Before these problems are solved, the exciting achievements in laboratory can be hardly transferred to industry for outdoor applications. In this Review, we focus on the recent studies on understanding the chemical instability of perovskite materials and the attempts by worldwide researchers to fabricating PSCs with stable PCE. The aim is to provide the reader some feasible approaches towards reasonably air-stable and high-PCE PSC devices for outdoor applications in near future.

2 Mechanisms of perovskite degradation and hysteresis phenomena in PSC

2.1 Thermal decomposition of perovskite

For most of the solution deposition techniques, a subsequent heat treatment is required. This has the dual purpose of removing any excess solvent remaining in the film as well as facilitating the formation of the perovskite crystal. The perovskite crystal material has been reported to be stable up to 300 °C,[63] at which point the organic component decomposes, leaving behind the inorganic PbI_2 through the following reaction:[18, 64]

$$CH_3NH_3PbI_3 \leftrightarrow PbI_2 + CH_3NH_2 + HI \quad (1)$$

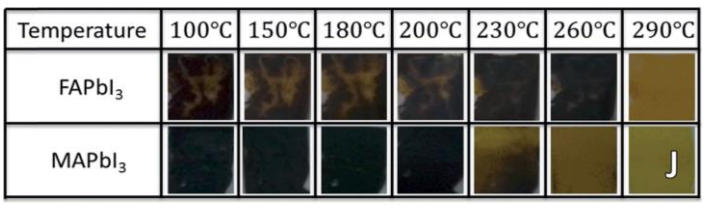

Fig. 4 Photographs of $MAPbI_3$ or $FAPbI_3$ films on glass after annealing at various temperatures. Reprinted from Ref. [65] with the permission from The Royal Society of Chemistry.

Etgar and co-worker considered that $MAPbI_3$ sample on glass started to decompose into PbI_2 at around 200 °C (see Fig. 4), judging from the yellow color emerging in the dark film.[65] However, this transformation may start to occur early at 140 °C according to Dittrich and co-workers.[66] Furthermore, Gratzel and Nazeeruddin demonstrated that 100 °C is an idea temperature for annealing the $MAPbI_3$ perovskite.[67] Samples that were annealed at 100 °C gave the highest PCE of 11.66%, but lower (<80 °C) or higher (>150 °C) annealing temperatures dramatically reduced the PCEs below 10%.

$FAPbI_3$ perovskite, which has been used in several kinds of PSC devices,[68-71] may sustain higher annealing temperatures (see Fig. 4). Snaith and co-workers employed $FAPbI_3$ as light harvester for planar heterojunction PSC and obtained high PCE up to 14.2%.[71] And Park et al developed the PCE using the blank polymorph $FAPbI_3$ and achieved efficiency up to 16.01%.[72] In both work, the samples were annealed at high temperatures (>140°C, at which $MAPbI_3$ starts to decompose). In comparison with $MAPbI_3$, the higher temperature tolerance ability of $FAPbI_3$ would demonstrate some advantages in future commercial applications.

2.2 The degradation of perovskite in ambient air

It's well known that the organic-inorganic halide perovskite is very sensitive to moisture and oxygen, so that the prepared perovskite film should be kept in glove box with the protection of inert gases.[52] Take $CH_3NH_3PbI_3$ for example, the detailed degradation steps in the presence of moisture can be illustrated by the following reactions:[73]

$$CH_3NH_3PbI_3(s) \overset{H_2O}{\longleftrightarrow} PbI_2(s) + CH_3NH_3I\ (aq) \quad (2)$$

$$CH_3NH_3I\ (aq) \leftrightarrow CH_3NH_2(aq) + HI\ (aq) \quad (3)$$

$$4HI\ (aq) + O_2 \leftrightarrow 2I_2(s) + 2H_2O\ (l) \quad (4\text{-}1)$$

$$2\mathrm{HI}(aq) \overset{hv}{\leftrightarrow} H_2(g) + I_2\ (s)\ . \quad (4\text{-}2)$$

By reacting with H_2O, solid state $CH_3NH_3PbI_3$ will firstly decompose into CH_3NH_3I solution and PbI_2 (reaction 2). Then, the CH_3NH_3I solution will continue decompose into CH_3NH_2

solution and HI solution (reaction 3). Thus, in the moisture, CH_3NH_3I, PbI_2, CH_3NH_2 and HI will co-exist in the perovskite film. The whole degradation process could be accelerated by the oxidation of HI in the presence of O_2 (reaction 4-1), or the decomposition of HI under UV radiation (reaction 4-2), leading to conversion of perovskite entirely to PbI_2.

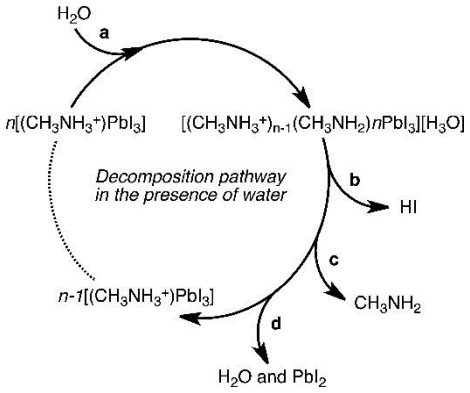

Fig. 5 Possible decomposition pathway of hybrid halide perovskites in the presence of water. Reprinted with permission from Ref. [74]. Copyright 2014 American Chemical Society.

Another similar decomposition pathway (Fig. 5) for $CH_3NH_3PbI_3$ has been proposed by Walsh and co-workers.[74] In the case of water exposure, water molecule, which is Lewis base, will combine with $CH_3NH_3PbI_3$ and take away one proton from ammonium, leading to the formation of intermediates $[(CH_3NH_3^+)_{n-1}(CH_3NH_2)nPbI_3][H_3O]$. These intermediates will subsequently decompose into CH_3NH_2, HI and finally into PbI_2 by the phase changes of both hydrogen iodide (soluble in water) and the methylammonia (volatile and soluble in water). Base on this simple reversible acid-base reaction, Zhu and coworkers also illustrated the temporary bleaching phenomenon of perovskite in the presence of another Lewis base ammonia.[75] Moreover, it was thought that hybrid perovskite incorporation aprotic organic ions, such as tetramethylammonium $(CH_3)_4N^+$, may be chemically stable in the presence of water.

2.3 The degradation caused by other parts of PSC device

Apart from the water and oxygen in ambient air, the using of certain materials in other parts of PSC might militate against the stability of perovskite. TiO_2, which is the typical photocatalyst for oxidizing water to create hydroxyl radicals and oxidizing organic materials,[76] has been used as the most common photoanode in PSC. However, Nishino and co-workers found that after the light exposure (AM1.5, 100 mW cm^{-2}) for 12 h, the original layer of $MAPbI_3$ turned into PbI_2, evidenced by the decreased light absorption spectra and

XRD patterns.[77] They proposed a possible mechanism to explain the degradation process under light exposure as followings:

$$2I^- \leftrightarrow I_2 + 2e^- [at\ the\ interface\ between\ TiO_2\ and\ MAPbI_3] \quad (5)$$

$$3CH_3NH_3^+ \leftrightarrow 3CH_3NH_2(\uparrow) + 3H^+ \quad (6)$$

$$I^- + I_2 + 3H^+ + 2e^- \leftrightarrow 3HI(\uparrow) \quad (7)$$

Since the $MAbI_3$ perovskite crystal is composed of $CH_2NH_3^+$, Pb^{2+} and I^- ions, TiO_2 can extract electrons from I^- and deconstruct the perovskite, leading to the formation of I_2 (reaction (5)). In the presence of water, the pK_a of the equation ($CH_3N_3^+ + H_2O \leftrightarrow CH_3NH_2 + H_3O^+$) is 10.80, which suggests that the equilibrium of reaction (6) should be proceed backward; however the elimination of H^+ through reaction (7) and evaporation of CH_3NH_2 drive the reaction (6) to forward. Hence, the electron extracted by TiO_2 can return to reduce I_2 through reaction (7), promoting the electron extraction at the TiO_2/$MAPbI_3$ interface as well as the formation of PbI_2 (see schematics in Fig. 6a). To deactivate the electron extraction at the TiO_2/$MAPbI_3$ interface, Nishino et al. inserted Sb_2S_3 layer as a blocking layer into the interface (see Fig. 6b). By doing this, the stability of the perovskite under light exposure was significantly enhanced.[77]

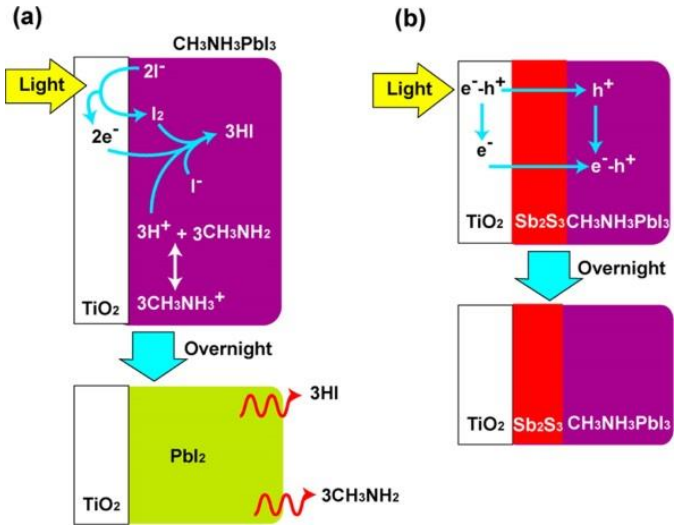

Fig. 6 Degradation scheme of MAPbI3 during UV light exposure test: (a) TiO_2/$MAPbI_3$ and (b)TiO_2/Sb_2S_3/$MAPbI_3$. Reprinted with permission from Ref. [77]. Copyright 2014 American Chemical Society.

Furthermore, Snaith and Steiner et al have found that solid-state DSSC devices based on mesoporous TiO_2 photoanode suffered from a rapid decay in power conversion efficiency under UV illumination.[78] And the same deterioration in performance also occurred in PSC devices.[79] They ascribed this deterioration to the defect states on mesoporous TiO_2 and suggested that oxygen is necessary for removing the surface states on TiO_2; Re-exposing the degraded devices to air led to a full recovery of the initial performance.

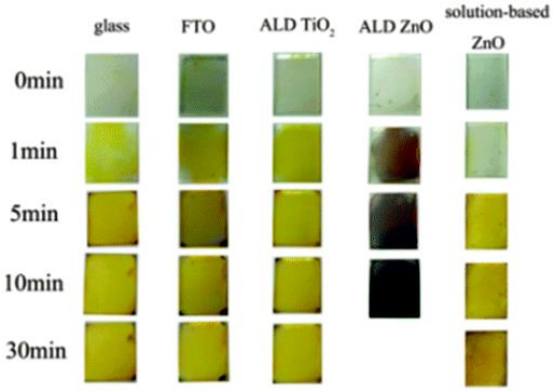

Fig. 7 Photographs of the perovskite films prepared with precursors containing CH_3NH_3I and $PbCl_2$ on different substrates and placed at room temperature in glove box with varying durations. Reprinted from Ref. [80] with permission from The Royal Society of Chemistry.

The interface issue causing deterioration also applies to ZnO. This has been systematically looked at by Dong et al. who deposited perovskite on various substrates from the precursor solution containing CH_3NH_3I and $PbCl_2$. It was revealed that ZnO film prepared by the atomic layer deposition (ALD) method can dramatically promote the formation of $MAPbI_3$ perovskite even at room temperature.[80] As shown in Fig. 7, the sample based on ALD-ZnO is the only one that changed its color to dark at room temperature, indicating the formation of perovskite. This "unusual" formation of perovskite film was proposed to occur by the following reactions:

$$3CH_3NH_3I + PbCl_2 \leftrightarrow CH_3NH_3PbI_3 + 2CH_3NH_3Cl \quad (8)$$

$$2CH_3NH_3Cl + ZnO \leftrightarrow 2CH_3NH_2 + ZnCl_2 + H_2O \quad (9)$$

$$ZnCl_2 + H_2O \leftrightarrow \mathrm{H}[ZnCl_2(OH)]. \quad (10)$$

At room temperature, the conversion to the perovskite is dominated by reaction (8), and the rate is very slow unless CH_3NH_3Cl is depleted.[67] In comparison to solution-ZnO, ALD-ZnO has a higher concentration of oxygen vacancies, leading to a great enhancement in its reaction

activity. Hence, ALD-ZnO can react readily with CH_3NH_3Cl (reaction (9)) and thus promotes the reaction (8). Although H_2O can be absorbed by $ZnCl_2$ through reaction (10), PSC devices employing this ALD-ZnO blocking layer together with the chloridion precursor still has a poor performance. This unfavorable reaction between ALD-ZnO and CH_3NH_3Cl should be taken into consideration when fabricating PSC based on chlorinated perovskite (such as $MAPBI_{3-x}Cl_x$).

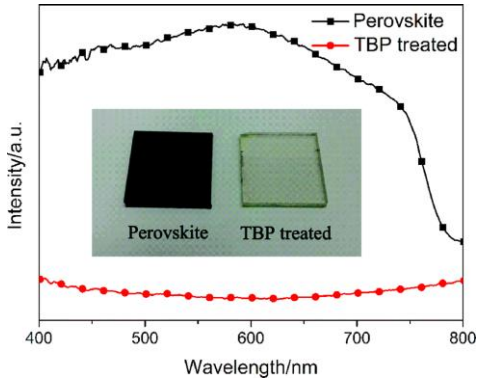

Fig. 8 UV-vis spectra and photo images of TiO_2/perovskite film and TBP-treated film. Reprinted from Ref. [81] with permission from The Royal Society of Chemistry.

Spiro-OMETAD,[41] which is the most commonly used HTM in PSC,[43, 52, 54, 59] generally needs addition of 4-tert-butylpyridine (TBP) to reduce charge recombination,[82] and bis(trifluoromethane)sulfonimide lithium salt (Li-TFSI) to increase its hole mobility.[83] However, several researchers found that the doping with Li-TFSI was highly dependent on the presence of oxygen atmosphere,[84, 85] which may lead to poor stability and reproducibility of the device. Even worse, Li-TFSI salt is extremely hygroscopic and deliquescent. Water molecular may easily penetrate into the PSC device without encapsulation, leading to the decomposition of perovskite. In addition, the acetonitrile, which is the conventional solvent for Li-TFSI, can also corrode perovskite.

Not only that, perovskite such as $MAPbI_3$ will deteriorate rapidly in the presence of TBP.[81] As shown in Fig. 8, the TiO_2/perovskite film clearly faded, with a sharp decrease in absorption intensity, upon the dropping of TBP under N_2 atmosphere. This process can be illustrated by following reactions:

$$CH_3NH_3PbI_3 \leftrightarrow CH_3NH_3I + PbI_2 \quad (11)$$

$$PbI_2 + xTBP \leftrightarrow [PbI_2 - TBP_x](solution) \quad (12)$$

$$PbI_2 + xTBP \leftrightarrow [PbI_2 \cdot xTBP](solid) \quad (13)$$

Firstly, $MAPbI_3$ decomposes into CH_3NH_3I and PbI_2 in a dynamic equilibrium (reaction 11), then TBP dissolves PbI_2 in a mass percentage of 7.75% at room temperature, forming PbI_2-TBP solution (reaction 12). In this process, TBP interacts with the center of Pb metal and formed a complex solid with pale-yellow color, *i.e.* [PbI_2·*x*TBP] (reaction 13), which has a different XPS feature from PbI_2.

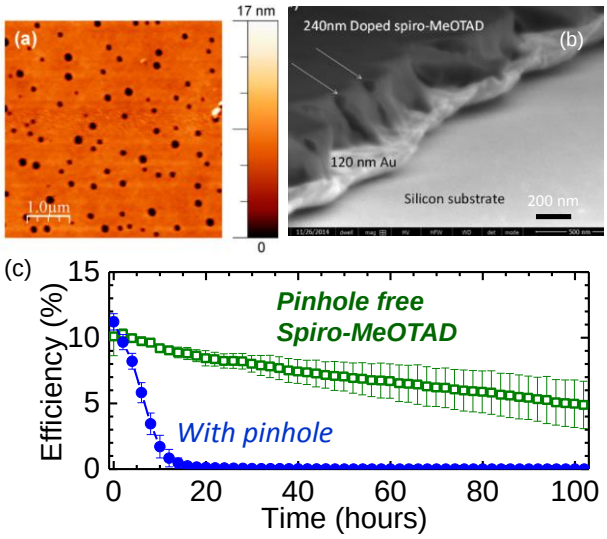

Fig. 9 Pinholes observed in spiro-MeOTAD films. (a) Tapping-mode AFM topography image of doped spiro-MeOTAD after 24 h air exposure. (b) Cross sectional SEM image showing the he pinholes running through the spiro film. Reprinted with permission from Ref. [86]. Copyright 2014 American Chemical Society. (c) Stability profile of the FTO/bl-TiO2/mp-TiO2/MAPbI3/spiro-MeOTAD/Au perovskite solar cell with spiro-MeOTAD dissolved in chlorobenzene (with pinhole) and chloroform (pinhole free) operated under air with controlled relative humidity of ~42%. Reprinted from Ref.[87] with permission from The Royal Society of Chemistry.

Apart from the additives of TBP and TFSI in spiro-OMETAD, the morphology of Spiro-OMETAD film also has an important effect on the stability of PSC device. Very recently, Qi and co-workers reported that small-sized pinholes commonly exist in spiro-OMETAD layers.[86] A large density of pinholes forming channels across the entire spiro film (~240 nm depth) can be observed (see Fig. 9a and b). These pinholes are likely the cause for the short life time for most PSC that use spin-coated spiro-OMETAD film as HTM. It was believed by

the authors that the pinholes not only can facilitate moisture migration through spiro-OMETAD film to reach the perovskite layer, but also can allow elements in the perovskite (e.g., iodine) to migrate to the top surface. Both cause degradation of the solar cell. To solve this problem, they changed the solvent of spiro-OMETAD from the commonly used chlorobenzene to chloroform and found that pinholes vanished in the spiro-OMETAD film. The stability of the device with such pinhole-free HTM is significantly improved (see Fig. 9c).[87, 88]

2.4 On the origins of hysteresis phenomenon in PSC device

Commonly, the PCE of a solar cell device is determined by exposing it to a standard AM 1.5G illumination with a power output of 1000 W m^{-2} and sweeping an applied bias across the terminals of the cell over a predetermined voltage range while measuring the current flowing in the external circuit. By doing this, a current-voltage (J-V) curve of the device can be obtained and from this curve, the device performance metrics of open-circuit voltage (V_{oc}), short-circuit current (J_{sc}) and fill factor (FF) are determined. This measuring process is intended to represent the steady-state power output of a solar cell at any given bias and should not be dependent on bias sweep rate or sweep direction. For most of the solar cells (including DSSCs, OPV and silicon cells), however, there may exist a slight difference in the shape of the J-V curves when fast sweeping from short-circuit to open-circuit (forward scan, FS) and form open-circuit to short-circuit (reverse scan, RS). The changes in the J-V curves measured by FS and RS methods, referred as hysteresis effect, typically arise from the capacitance effect of the solar cell device. Specifically, when the scanning rate is fast, the solar cell can be charged up under RS condition, and the extra-capacitive charges together with the photogenerated charges can be both extracted, causing an increase in J_{sc}. On the contrary, the photogenerated charges can partially charge the solar cell under quick sweeping by FS method, causing a reduction of the J_{sc}. Coming to perovskite solar cells, however, the detailed reasons may differ and still not absolute clear, but may vary from device to device. In the following we discuss a few examples.

Early in 2013, Grätzel group has investigated the PSC device with a structure evolving from solid-state DSSCs (Fig. 2b) by impedance spectroscopy (IS).[89] They found a strong hysteresis in the J-V curves under illumination, which manifests mainly only in the FS procedure. The PCE value obtained by FS method is strongly dependent on the scan speed, indicating that some slow charged carriers are involved in the current and voltage generation. By using IS measurement, they observed a slow time constant phenomena in the Nyquist plot

of a standard device under illumination. Even in the device without HTM, this phenomenon was also observable. They deduced that such slow process may mainly arise from the ionic charge transport, ion intercalation, or the ferroelectric effect[18] of perovskite material. Snaith group have also shown an anomalous hysteresis present in the J-V curves of PSC, and the specific device architecture influences the severity of the hysteresis.[90] Moreover, unlike what would be expected from typical capacitive charging and discharging effects, the hysteresis turned more extreme as the scan rate was reduced; and even at extremely slow scan rates there still appeared a significant hysteresis. They suggested three possible origins: (i) The large defect density within or near the surface of perovskite or specifically generated interface states. (ii) The ferroelectric properties of perovskite materials. (iii) Excess ions as interstitial defects present in and predominantly labile throughout the perovskite film.

Walsh and co-workers reported a model describing the molecular orientation disorder in $CH_3NH_3PbI_3$.[91] By electronic structure calculations, they investigated the temperature and static electric field dependence of the equilibrium ferroelectric domain structure and resulting polarizability. A rich domain structure of twinned molecular dipoles can be observed, which varies strongly as a function of temperature and applied electric field. Hence, they proposed that the internal electrical fields associated with microscopic polarization domains contribute to hysteretic anomalies in the J-V response of PSC device. Similar results have also been reported by Yu group[92] and Miyasaka group[93]. Obviously, the ferroelectric properties of the perovskite materials could be one important origin of hysteretic effect for PSC, but not the sole one.

The trap states on the surface and grain boundaries of the perovskite materials could be another origin of hysteresis effect in PSC with planar structure, according to Huang.[94] They used thermal admittance spectroscopy (TAS) analysis to quantize the trap states in perovskite films by the passivation of Phenyl-C61-butyric acid methyl ester (PCBM). The results showed that the trap density of states decreased dramatically by coating the PCBM on the perovskite films, leading to a significant lowering of the photocurrent hysteresis. On the basis of this, Dong and co-worker[95] also reported that both in porous and planar structure PSC device, the current hysteresis can be explained by the dynamic charge trapping-detrapping processes.

In addition to charge trapping-detrapping, ion migration in perovskite has also been identified as possible reason. By combined computational and experimental study, Islam and O'Regan provided new atomic-scale insights into the ion transport mechanisms operating in

the hybrid perovskite $CH_3NH_3PbI_3$.[96] They found a facile vacancy-assisted migration of iodide ions with an activation energy of 0.6 eV, which is in good agreement with activation energies derived from kinetic measurement on $CH_3NH_3PbI_3$-based PSC device. Such ion migration has been suggested as a factor contributing to the unusual behavior of PSC, including hysteresis in J-V curve[89] and a giant dielectric[97] response at low frequencies. Moreover, Gregori and Maier[98] also reported that the ionic conductivity of perovskite $CH_3NH_3PbI_3$ is higher than the electronic conductivity. This ion migration, according to Unger and McGehee,[99] could not only cause the hysteresis effect but is also likely detrimental to the long-term reliability of PSC device.

Recently, the structural changes of perovskite material under illumination or bias have been reported by several groups.[100] Under light and bias, the methylammonium ions ($CH_3NH_3^+$) have enhanced rotational freedom and may align with the electric field. This alignment might be very fast, but the adjustment of the inorganic scaffold is much slower. Indeed, Sum and Mathews[101] investigated PSC devices by electro-optical study and found a structural response of the $CH_3NH_3PbI_3$ perovskite that involves a complex interplay between the lattice/$CH_3NH_3^+$ ions and applied E-field/charge accumulation. They believed that such charge accumulation due to inefficient charge transfer will strongly distort the perovskite structure and cause the pronounce hysteresis.

In sum, anomalous hysteresis has a detrimental influence on the reliability and stability of PSC devices. Although different origins to such behavior have been proposed, there still was no solid evidence to support these proposed mechanisms. For the future development of PSC, it is a challenge and indispensable to find effective approaches to circumvent the hysteretic and degradation problems of perovskite, which is equally important to striving for higher power conversion efficiencies.

3. Strategies in improving the stability of PSC

The traditional perovskite cell consists of a lead halide perovskite $CH_3NH_3PbI_3$ sensitizers, which are loaded into a mesoporous TiO_2 layer, and a hole transport layer spiro-OMeTAD with LiTFSI and TBP as dopants. Typical attempts to enhance the stability of perovskite solar cells include modification of the perovskite sensitizer, modification of the additives in hole transport material, using polymers as hole transport materials, using

inorganic hole transport materials, using inorganic hole transport materials, and hole-conductor free PSC. These strategies will be elaborated as follows.

3.1 Modification of the components in traditional PSC

3.1.1 Modification of the perovskite sensitizer

Perovskites have an AMX_3 formula in general crystal structure which is a combination of two cubic geometries with 8 cations A located at eight vertexes of an M-centered cube. Cation M is also the center of an octahedron forming by 6 anions X which located at the centers of six faces of the M-centered cube (see Fig. 1). Organic-inorganic perovskites, where A is an organic cation, are of special interest in the perovskite families due to their unique structures, where inorganic components are intercalated by organic components on the molecular scale. These organic-inorganic perovskites are particularly interesting due to their distinctive optical and electronic properties, where the organic layers help to specify the degree of internal interactions as well as the electronic properties in the inorganic layers.[29]

The cubic structure of perovskite can be changed to orthorhombic or rhombohedral structures when cations A and M are replaced by other elements. These structural distortions will affect electric and optical properties of perovskite. In addition, the size of cations A and X will also influence the lattice structure leading to change in the properties of the perovskite.[102] It is also possible to greatly enhance the stability of perovskite by controlling the composition without sacrificing the cell performance.[102-104]

Modification of the traditional perovskite sensitizer $CH_3NH_3PbI_3$ have been conducted by the Seok group in 2013.[103] In this paper, based on the fact that $MAPbI_3$ is more sensitive to moisture compared with $MAPbBr_3$,[102, 105] the Br substitution ratio for I in the perovskite $MAPb(I_{1-x}Br_x)_3$ was changed with x = 0, 0.06, 0.20, and 0.29. The cells were exposed to relatively high humidity (55%) for one day while keeping the humidity to 35% on the other days. It was found that, the solar cells fabricated with $MAPb(I_{1-x}Br_x)_3$ were all more stable compared with the traditional composition $CH_3NH_3PbI_3$, among which the one with x = 0.2 gives the highest efficiency and stability within 20 days (see Fig. 10a). Interestingly, at the composition of x = 0.20 and 0.29, the cells showed a tendency of increase in PCE in the first 6 days, for which the mechanism was not clear.

Similarly, the iodide-chloride mixed-halide perovskite $CH_3NH_3PbI_{3-x}Cl_x$ was also remarkably stable during processing in air. The absorption spectra (Fig. 10b) demonstrated good light-harvesting capability over the visible to near-IR range. And the absorption spectrum maintains its profile over 1000 h constant illumination by simulated full sunlight.[106]

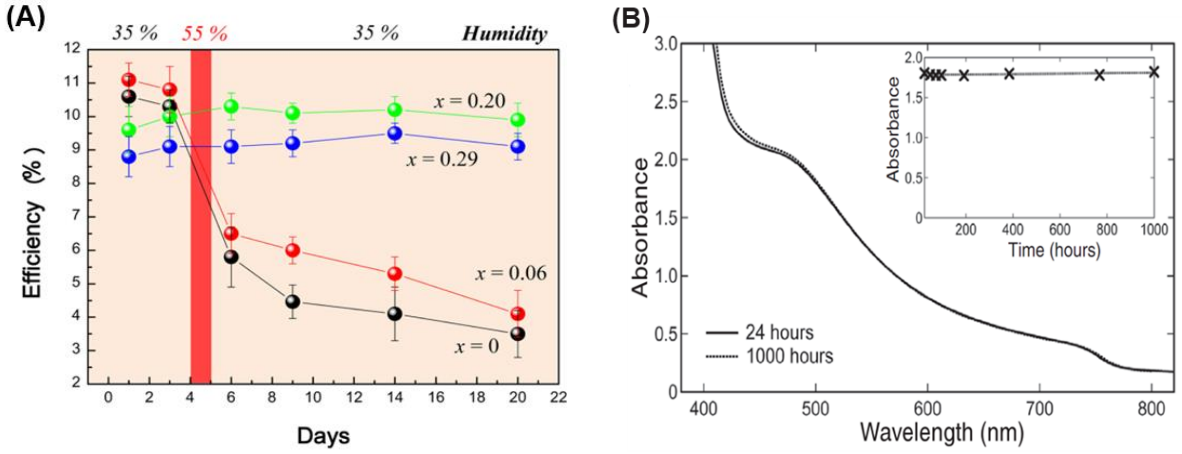

Fig. 10 (A) Power conversion efficiency variation of the heterojunction solar cells based on $MAPb(I_{1-x}Br_x)_3$ with time of storage in air at room temperature without encapsulation. The humidity was varied at different periods. The cells with x = 0.2 has the best stability after 20 days.[103] (B) Ultraviolet to visible (UV-Vis) absorption spectra of the photoactive layer in the solar cell (mesoporous oxide + $CH_3NH_3PbI_{3-x}Cl_x$ perovskite absorber + spiro-OMeTAD). Inset is the absorbance as a function of time up to 1000 h exposure to simulated AM1.5 sunlight at 100 mW cm^{-2}.[106]

In addition to the compounds of lead halide perovskite ($MAPbCl_3$, $MAPbBr_3$, $MAPbI_3$) which have been long studied, the compounds of the formulas $(C_6H_5(CH_2)_2NH_3)_2PbX_4$ and $(CH_3NH_3)(C_6H_5(CH_2)_2NH_3)_2Pb_2I_7$ (where X = Cl, Br, I) and similar with $C_nH_{2n+1}NH_3$ or $H_3NC_nH_{2n}NH_3$ (n = 4,6,8,9,10...) instead of $C_6H_5(CH_2)_2NH_3$, have been prepared and their 2-D semiconducting behavior has been established.[107] In $(C_6H_5(CH_2)_2NH_3)_2PbI_4$ the 2-D network of PbI_4 form perovskite anion components, while alkylammonium chains play the role of cations. Also, in $MA(C_6H_5(CH_2)_2NH_3)_2Pb_2I_7$ the cation/anion (MA/Pb_2I_7) layers alternate with cation ($C_6H_5(CH_2)_2NH_3$) layers.

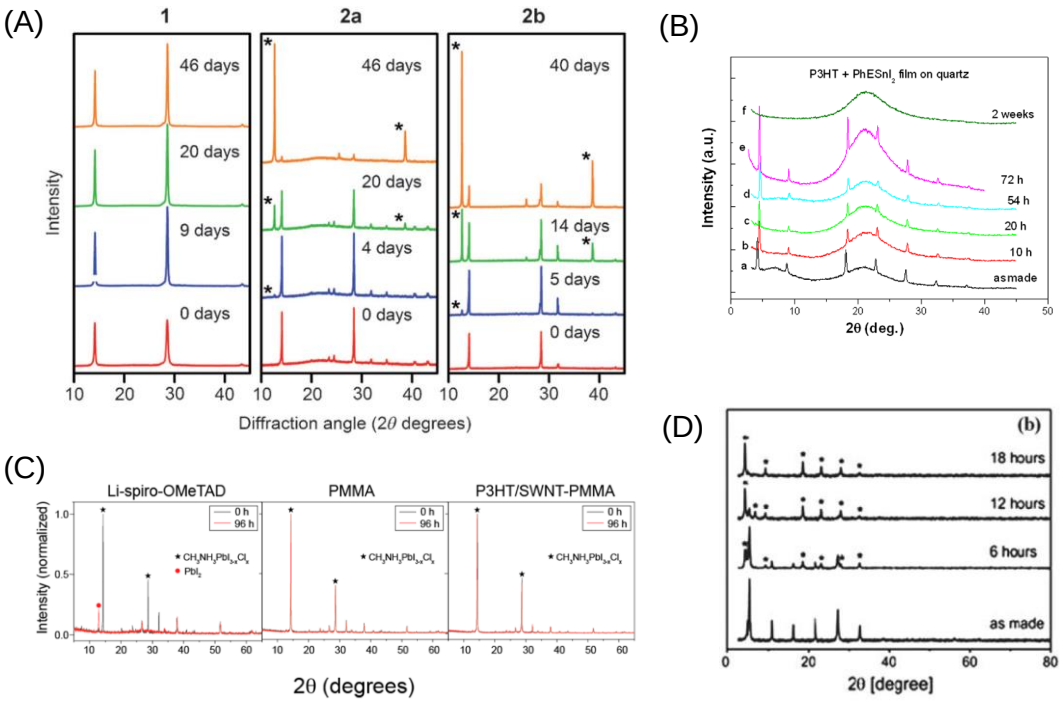

Fig.11 (A) X-ray diffraction patterns of films of $(PEA)_2(MA)_2[Pb_3I_{10}]$ (1), $(MA)[PbI_3]$ formed from PbI_2 (1a), and $(MA)[PbI_3]$ with 1:3 molar ratio of $PbCl_2$:(MA)I (2b), which were exposed to 52% relative humidity. Annealing of films of 2a for 15 min and 2b for 80 min was conducted at 100 ^oC prior to humidity exposure. Asterisks denote the major reflections from PbI_2.[108] (B) Spin-coated $(PEA)_2SnI_4/P_3HT$ blend film on quartz substrate expose to air for different periods. (C) XRD patterns of devices with three types of hole transport layers (Li-spiro-OMeTAD, PMMA, and P3HT/SWNT-PMMA) before (black line) and after (red line) 96 h heat exposure.[109] (D) The spin-coated film of the pure $(PEA)_2SnI_4$ exposed to air for different periods.[102]

It is known that lead halide perovskites degrade easily in the presence of moisture because of the hygroscopic amine salts which greatly limits their practical applications. Changing alkylammonium groups from the CH_3NH_3 to longer and more hydrophobic chains such as $C_6H_5(CH_2)_2NH_3$ or $(C_6H_5(CH_2)_2NH_3)_2(CH_3NH_3)_2$ can improve the stability of perovskites; For example, in the work by Smith et al. the solar cell using $(C_6H_5(CH_2)_2NH_3)_2(MA)_2[Pb_3I_{10}]$ was stable upon exposure to a relative humidity of 52% at room temperature for 46 days without appearance of additional peak in the XRD pattern (see Fig 11A), and PCE was around 7%.[108]

For tin-based halide perovskites, the stability is also a major issue to be solved.[110] In fact, the compounds of tin halide perovskite with formulas $(C_nH_{2n+1}NH_3)_2SnX_3$ and (CH_3NH_3) $(C_nH_{2n+1}NH_3)_2Sn_2I_7$ have been prepared in powder form and their optical

properties have been reported by the Papavassiliou group since 1990's.[107] The narrow excitonic absorption and luminescence bands are characteristic features of this kind of tin-based perovskites. In this paper the preparation of $(C_6H_5(CH_2)_2NH_3)_2SnI_4$ and $(C_6H_5(CH_2)_2NH_3)_2SnBr_4$, in pure crystalline form, as well as their analytical and spectroscopic data are reported. The blend film was prepared by adding P3HT to the $(C_6H_5(CH_2)_2NH_3)_2SnI_4$ precursor solution in tetrahydrofuran (THF) and spin coating. As seen from XRD profiles (Fig. 11B), the layered structure of $(C_6H_5(CH_2)_2NH_3)_2SnI_4$ was kept in air for at least 72 h. In comparison, the pure $(C_6H_5(CH_2)_2NH_3)_2SnI_4$ film decomposes within several hours in air (Fig. 11D).[102]

3.1.2 Modification of the additives in hole transport material

Since the conventional used additives of LiTFSI and TBP in spiro-OMETAD have negative effect for the stability of perovskite, exploring other kinds of HTM and doping materials is one popular way to improve the stability of PSC. In the study by Zheng and co-workers, a highly hydrophobic oligothiophene derivate named DR3TBDTT, which contains a central alkoxy-substutited benzo[1,2-b:4,5-b']dithiophene (BDT) unit and thiophene at the 4- and 8-positions, was used in an attempt of introducing an "additive-free" HTM (without LiTFSI and TBP).[111] In doing so, they obtained the efficiency of 4.9%. Then, by adding a new additive of PDMS, the efficiency was increased to 8.8%, close to that (8.9%) of control $CH_3NH_3PbI_{3-x}Cl_x$ cell (see Fig. 12A). Interestingly, for 3 days exposure in 50% relative humidity, the DR3TBDT/PDMS based perovskite cell demonstrated improved stability with respect to the traditional cell; the efficiency reduced from 8.8 to 8.0% compared to the reduction from 8.9 to 3.9% of the control device (see Table 1). The DR3TBDTT films also showed a very large water contact angle of 107.41°, which is beneficial because a hydrophobic hole transport layer can effectively prevent the water penetration into the perovskite layer (see Fig. 12B).

Table 1. The efficiency stabilities of perovskite cells from J-V measurements under standard AM1.5 illumination (100 mW cm^{-2}) of devices with different relative humidity. Adapted from Ref.[111]

Additives to HTM	After 13 days in 20% humidity	After 3 days in 50% humidity

Spiro-OMeTAD+Li-TFSI +tBP	8.3% → 7.7%	8.9% → 3.7%
DR3TBDT+Li-TFSI +tBP	3.3% → 3.1%	3.7% → 0.9%
DR3TBDT		4.9% → 4.4%
DR3TBDT + PDMS		8.8% → 8.0%

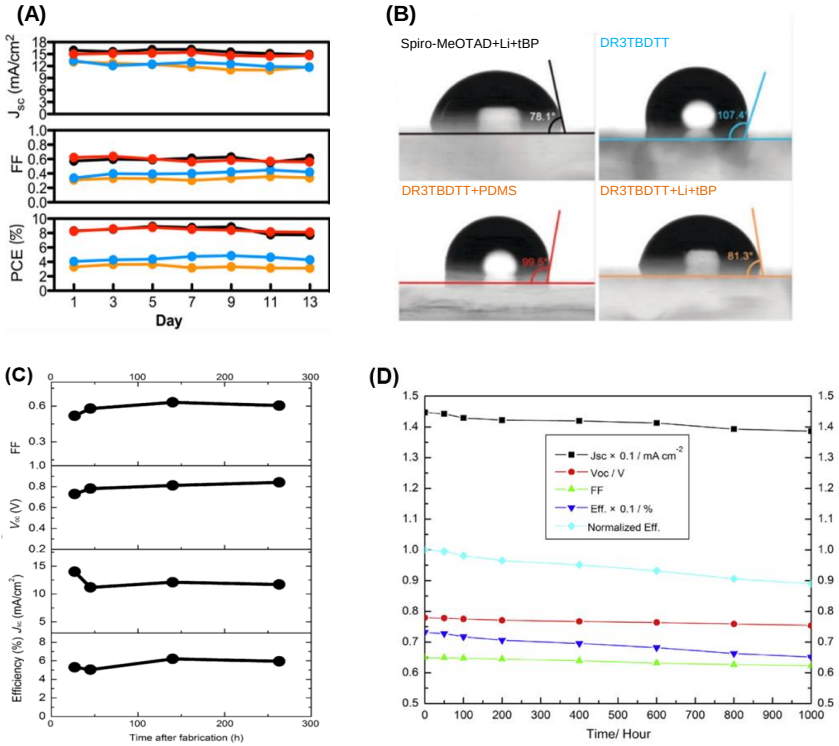

Fig. 12 (A) Evolution of photovoltaic parameters of devices using DR3TBDTT, DR3TBDT + PDMS, DR3TBDT+Li-TFSI +tBP, and Spiro-OMeTAD+Li-TFSI +tBP as the HTM under 100 mW cm^{-2} simulated AM1.5G. Cells were stored in air at room temperature in the dark (humidity <20%). (B) Water contact angles of each HTM films on a glass substrate;[111] (C) Stability of $CH_3NH_3PbI_2Br$/P3HT cells stored in air at room temperature which retains a PCE of around 6.6% after 250 h;[112] and (D) Time-course changes of the normalized efficiency and photovoltaic performance of the devices using PANI. The initial PCE of 7.34% reduces to 6.71% after 1000 h under 100 mW cm^{-2}.[113]

In an attempt to use dopant-free hole transport material, tetrathiafulvalene derivative (TTF-1) was used by Liu et al.[114] With an PCE of 11%, the duration of solar cell was increased three times (360 h) in air at a 40% relative humidity compared to the traditional spiro-OMeTAD based cell (120 h).

Recently, Li et al. presented the result of decreasing the detrimental impact of TBP on perovskite.[81] In this work, a montmorillonite (MMT) layer was introduced on the perovskite surface, which, according to the authors, can absorb TBP into its intercalated structure and thus inhibits the direct contact of TBP with perovskite. As a result, the perovskite solar cell becomes more stable. Moreover, MMT can also limit charge recombination in the cell which leads to a PCE of 11.9% for the MMT-based cell compared to 9 % of the cell without MMT.

3.2 Polymer as the hole transport material

Another drawback that may limit perovskite solar cells to fulfill the rigorous international standards for outdoor photovoltaic applications is the high cost of spiro-MeOTAD (see Table 2). The fact is that since the birth of the first perovskite solar cell, the exploration for cost-effective HTMs has never been stopped.

Table 2. Cost comparison of HTM materials for different cell configurations.[112]

Device structure	Light absorber	HTM	Concentration$_{(HTM)}$ [mg mL^{-1}]	Cost$_{(HTM)}$ mL^{-1} [AU $]
Mesoscopic	$CH_3NH_3PbI_3$	Spiro[115]	72.3	93
Mesoscopic	$CH_3NH_3PbI_{3-x}Cl_x$	Spiro[116]	88 (8 wt. %)	113
Planar	$CH_3NH_3PbI_3$	Spiro[117]	180	231
Mesoscopic	$CH_3NH_3PbI_3$	Spiro[42]	208 (0.170 M)	267
Nanowire	$CH_3NH_3PbI_2Br$	Spiro[118]	208 (0.170 M)	267
Mesoscopic	$CH_3NH_3PbI_3$	P3HT[119]	15	12
Planar	$CH_3NH_3PbI_{3-x}Cl_x$	P3HT[120]	16.6 (1.5 wt. %)	13
Mesoscopic	$CH_3NH_3PbI_3$	P3HT[121]	20	16
Mesoscopic	$CH_3NH_3PbI_2Br$	P3HT[112]	10	8

Recently, Zhang et al. reported a work which solved both stability and cost issue of perovskite solar cells.[112] In this work, a dopant-free P3HT was used as the cheaper HTM as replacement of spiro-MeOTAD. In the meantime, the perovskite sensitizer, $CH_3NH_3PbI_2Br$, is also more stable in moisture than the $CH_3NH_3PbI_3$ sensitizer. As a result, the solar cells without any encapsulation can retain the efficiency of about 6.6% after exposing for 250 h in air (see Fig. 12C), which is considered fairly good in practical consideration.

Xiao and co-workers reported a new solar cell design using polyaniline (PANI) as a hole transport material in May 2014.[113] PANI in this design can function as both sensitizer and hole transport material. In doing so, solar cell based on the PANI delivers a conversion efficiency of 7.34%, and reduces to 6.71% after 1000 h, corresponding to an efficiency retention of 91.42% (see Fig. 12D).

In 2014, the Snaith group carried out a study on improving the stability of PSCs by coating carbon nanotube/polymer composites as the hole transport layer.[109] In this paper, under a temperature of 80 ^{o}C in atmostpheric condition, the PSCs with conventional hole transport materials (spiro-OMeTAD, P3HT, and PTAA) degraded significantly resulting in the color change to yellow. Interestingly, for the cells with Li-TFSI doped spiro-OMeTAD, the degradation was faster than the cells with undoped spiro-OMeTAD. It was explained that the additive Li-TFSI, which increases the hole tranfer ability of the HTM, plays also a negative role in introducing water into the cell, thus accelerates the cell degradation. In order to retard the degradation, an insulating poly(methyl methacrylate) (PMMA) polymer was used. The results showed that PMMA could act as an effective protective layer and the degradation was insignificant (Fig. 11C). However, the insulating PMMA is an unsuitable charge transport material. Therefore, single-walled carbon nanotubes (SWNTs), together with P3HT, were mixed with PMMA. In doing so, the composite P3HT/SWNTs and PMMA exhibited the protective ability and the thermal degradation was retarded. The obtained PCE was up to 15.3% with an average value of 10 ± 2%. In addition, the water-resistance of the cell is remarkably improved by using such hole-transporting and protective composite. Impressively, the cell could also run after being placed in water for 60 s. This work represents a critical advance in long-term stability, high-efficiency perovskite solar cells.

3.3 Inorganic hole transport material and surface treatment

Due to the high cost of spiro-OMeTAD (price ten times higher than Au and Pt), researchers attempt to employ inorganic hole transport materials. In the work by Christians et al., CuI was used as the hole conductor layer.[122] Inorganic material CuI is cheap, stable, solution-processable and have suitable band edges for perovskite solar cell. The PSCs employing CuI as HTM showed a champion efficiency of 6.0%, which is very close to that of the device based on spiro-OMETAD (7.9%). Moreover, under constant AM 1.5G

illumination for a period of 2 h, the current of CuI device kept its initial value while the spiro-OMETAD one decreased by approximately 10%.

Using inorganic oxides layer to treat the surface of the photoanode is a feasible way to enhance both the stability and the performance of solar cell. Many studies have described that some thin oxides films (such as Al_2O_3, SiO_2, ZnO, etc) can be used as a protective layer for the photoanode in DSSCs.[123-127] For the liquid-state DSSCs, the main effect of such oxide protective layer is suppressing the charge recombination. As shown in Fig. 13 A, the oxide protective layer (Al_2O_3) possesses a higher conduction band than the TiO_2, so that the electrons are injected to TiO_2. As a result, the charge recombination between TiO_2 and the electrolyte can be suppressed.

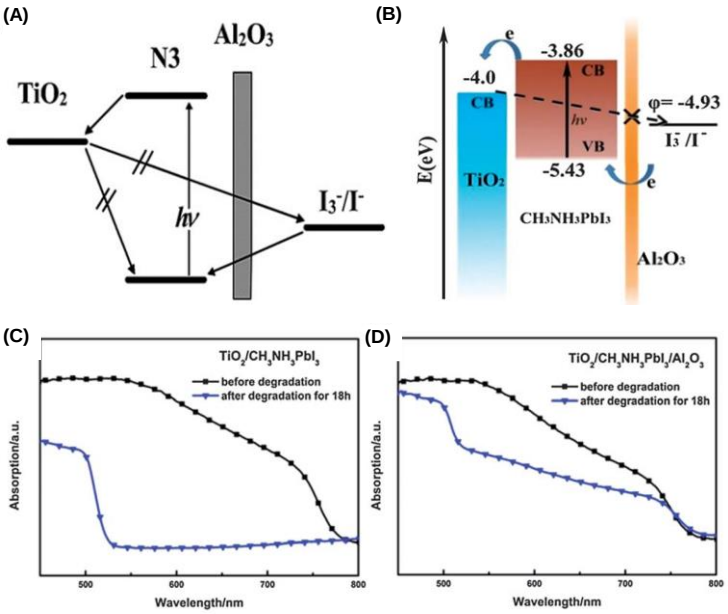

Fig. 13 (A and B) Illustration of the interfacial charge transfer processes occurring at the TiO_2/dye (or perovskite)/Al_2O_3/electrolyte interface of a DSSC. Repritned with permission from Ref.[124, 126] The light absorption of perovskite sensitized films (C) without Al_2O_3 and (D) with Al_2O_3 before and after degradation for 18 h. Repritned with permission from Ref. [128].

Evolving from the above idea in DSSCs, Li et al. also introduced a protective layer in PSCs.[126] They dipped the as-prepared TiO_2/perovskite film into a solution of aluminumtriethyl ($Al(C_2H_5)_3$ 25% w/w in hexane) and find that the perovskite sensitizer can be prevented from the electrolyte corrosion. The PCE of device showed a remarkable enhancement from 3.56% to 6.12%. In a follow-up work, the authors also applied the same Al_2O_3 protection in solid-state perovskite solar cells by coating the Al_2O_3 layer prior to the HTM Spiro-MeOTAD layer (see Fig. 13B).[128] The light absorption of perovskite sensitized

films was shown in the Fig. 13 C and 13D. Under sunlight illumination and 60% humidity for 18 h, the absorption of the Al_2O_3-modified perovskite cell still maintained to certain degree after degradation. In contrast, the absorption of the cell without protective layer decreased sharply. In this device, the Al_2O_3 layer plays two roles: protects the perovskite film from humidity and sunlight, and retards the electron recombination between HTM and TiO_2.

In addition to dielectric materials for stabilization of PSC, metals have been also applied recently by Da and co-workers, who sputtered Co, Cr and Ni layers on top of 80 nm Au layer of a conventional PSC cell.[129] It is found that the PSC with 8 nm Ni layer on top the Au cathode maintains an evidently more stable power conversion efficiency (around 12%) than bare PSC after storage in ambient environment (reduced from about 12% to 9%) for 12 days. This improved stability also allows the authors to assemble a PSC + Fe_2O_3 photoanode tandem cell for photoelectrochemical water splitting. With the device with an 8 nm Ni layer as the photoanode, the photocurrent density and stability were both remarkably improved: 56% retention of its original photocurrent after 100 sec of photoelectrochemical test under continuous chopped light illumination and a photocurrent density of ~2 mA cm^{-2} after 15−20 min PEC measurement in an alkaline solution. In this case, it is believed that Ni acts both protective layer of the $CH_3NH_3PbI_3$ and also catalyst for water oxidation reaction. Nevertheless, it is still obviously a great challenge to apply PSC in photoelectrochemical water splitting; probably a more viable way is to combine the PSC with electrocatalysts, as demonstrated by the Grätzel group.[130]

3.4 Hole-conductor free PSC

Since the additives such as lithium salt and TBP in most organic HTMs militate against the stability of perovskite, one solution is to design HTM free PSCs. Etgar and co-workers firstly demonstrated PSC devices that work properly without conventional additional HTM.[45] In this device (see Fig. 2e), the perovskite layer, which was contacted directly by the Au counter electrode, functioned as both light absorber and HTM at the same time. Holes that are excited at the perovskite/TiO_2 interface can be transported by the perovskite semiconductor and collected by the Au electrode, forming photocurrent. Under the standard AM1.5 illumination, such PSC showed a PCE of 5.5%. Soon after that, they improved the PCE up to 10.85% by employing sequential deposition method.[131] This novel type of PSC without extra HTM showed a promising future to tackle the stability problems caused by HTM, though the PCE need further improvement.

Recently carbon counter electrodes becomes popular in hole-conductor free PSCs. This direction was pioneered in Han group in Wuhan who obtained an initial PCE of 6.6% under standard AM1.5 illumination (see Fig. 2g and 14).[56] By using sequential deposition method, they gradually pushed the PCE up to 12.9%.[70, 132, 133] It should be noted that this carbon-based PSC without encapsulation were fabricated in air ambient (not glove box) and showed excellent stability in dry air. Apart from the absence of organic HTM, the unique triple-layered structure with all mesoporous components may be an important factor to the device stability of this carbon-based PSC. Different from the Au-based PSC, the filling process of perovskite material was done after the fabrication of carbon electrode. This prevents the exposure of perovskite directly to ambient atmosphere after its formation. Moreover, TiO_2 layer in this device was covered by an insulating ZrO_2 spacer layer, which may also protect the perovskite/TiO_2 layer from moisture to a certain degree.

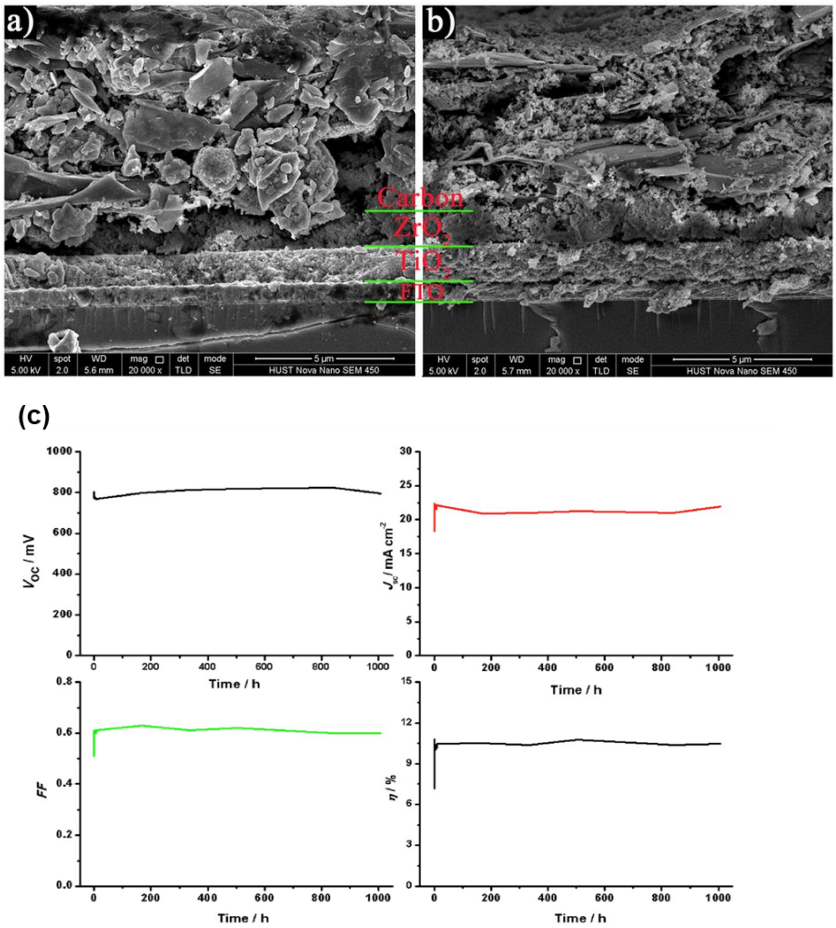

Fig. 14 Cross-sectional structure of carbon-based PSCs. (a) Spheroidal graphite-based device. (b) Flaky graphite-based device. Reprinted with the permission from Ref. [56]. Copyright 2013

Nature Publishing Group; (c) Stability test of a triple layer $(5\text{-AVA})_x(MA)_{1-x}PbI_3$ perovskite sensitized mesoscopic solar cell effected in full AM 1.5 simulated sunlight in ambient air over 1008 hours with an unsealed device, the perovskite being protected by the carbon layer acting as back contact. Reprinted from Ref. [57] with the permission of the American Association for the Advancement of Science, copyright 2014.

Still the carbon-based PSC structure need going one step further, the Han group reported a higher and certificated PCE of 12.8% by tailoring the composition of the perovskite.[57] By adding 5-ammoniumvaleric acid (5-AVA) iodide into the precursor of $MAPbI_3$, they obtained a new perovskite with the formula of $(5\text{-AVA})_x(MA)_{1-x}PbI_3$. It was shown that $(5\text{-AVA})_x(MA)_{1-x}PbI_3$ perovskite tends to align along its c axis. In comparison to the conventional $MAPbI_3$ perovskite, the unordinary alignment of $(5\text{-AVA})_x(MA)_{1-x}PbI_3$ perovskite makes its coating on TiO_2 surface much more uniform. As a result, the assembled PSC showed an excellent PCE and impressive stability (>1000 h) in ambient air under full sunlight (see Fig 14c).

Further improvements to this type of carbon-electrode, hole-conductor free PSC device have been achieved by other groups.[134-136] Wang and co-workers developed this hole-conductor-free PSC by adding a hole selective NiO contact between the ZrO_2 space layer and carbon layer, and enhanced the PCE of the device up to 14.9%.[137] Moreover, Meng and co-workers also reported a PCE of 13.53% in such hole-conductor-free PSC with free-standing flexible carbon electrode.[138] It is worth noting that the J-V curves of the forward and reverse scans are well coincident, indicating a week hysteresis effect. Considering the low-cost of the carbon electrode, this type of air-stable hole-conductor free PSC may hold a good potential for commercialization.

3.5 Hysteresis-free PSC

As mentioned in section 2.4, the anomalous hysteresis effect during J-V measurement have been observed in most PSC devices with different structures, which can cause both over- and underestimated efficiency values. Hence, producing hysteresis-free devices with sustainable performance seem to be essential for future development of stable PSC devices. Although the origin of such anomalous hysteretic effect is still unclear, several approaches that can effectively restrain the hysteresis to certain degree have been reported. These techniques include modification of the synthesis condition and precursor type (for planar PSC devices), and the N-type contact (for mesoscopic devices).

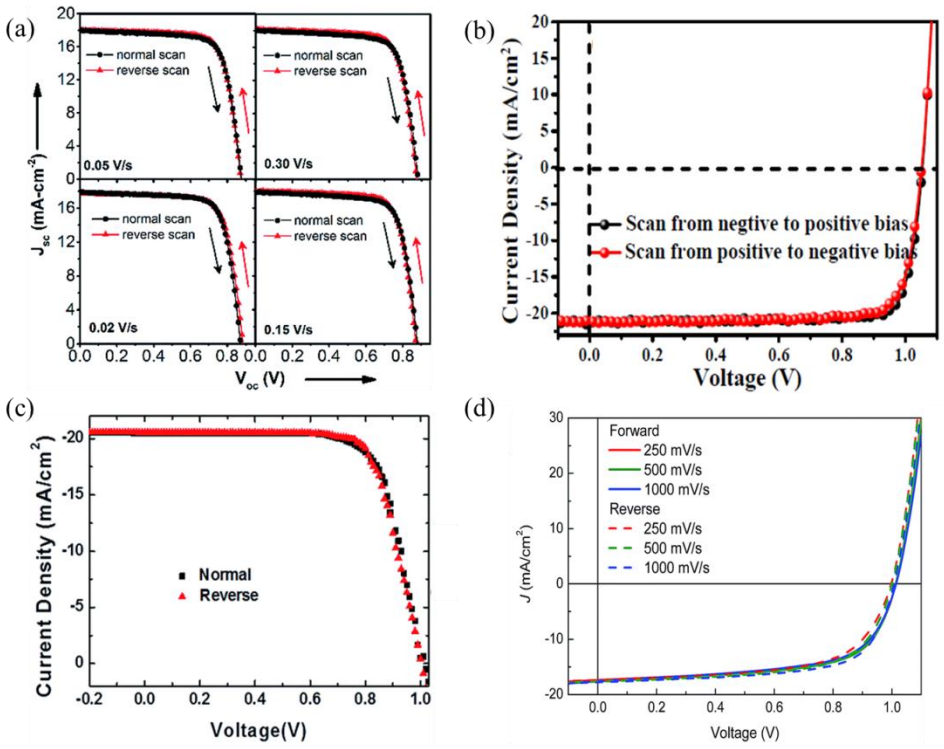

Fig. 15 Hysteresis-free J-V curves measured form different planar PSC devices: (a) PSC based on Cl-doped $MAPbI_{3-x}Cl_x$ perovskite; Reprinted with the permission from Ref. [141] (b) PSC based on H_2O treated perovskite; Reprinted with the permission from Ref. [142] (c) PSC fabricated by gradual annealing process; Reprinted with the permission from Ref. [143] (d) PSC fabricated by using lead acetate as the perovskite precursor. Reprinted with the permission from Ref. [144]

Since PCBM has been reported as an effective N-type contact for perovskite, PSC devices based on PCBM seemed have relatively weak hysteretic effect in comparison with other planar devices.[94, 101, 139, 140] In addition to PCBM as electronic contact, additional strategies have been developed to eliminate the hysteresis in planar PSCs. Shirai group[141] has demonstrated that the morphology of perovskite can be optimized by adding a small amount of methyl ammonium chloride (MACl) to the methyl ammonium iodide (MAI) solution in the inter-diffusion process. By doped with Cl, the perovskite films become smoother and more stable. As a result, the PSC device based on such Cl-doped $MAPbI_{3-x}Cl_x$ perovskite showed hysteresis-free J-V characteristics (see Fig. 15a) and excellent long-term stability. Similarly, Gratzel together with Wu, Nazeeruddin and Hagfeldt[142] also reported a strategy to synthesize high quality perovskite films. They added a few percent of H_2O into the PbI_2/DMF to make a homogeneous solution, and found that the PbI_2 film prepared from such homogeneous precursor solution is highly smooth and crystalline. The perovskite film

fabricated form this highly quality PbI_2 is extremely pure and dense without pinhole, resulting in a high PCE of 18% in PSC device without evident current hysteresis (see Fig. 15b).

Choy, Wong and Liao[143] reported a gradual annealing process with relative low temperatures (60–80 ºC) to form the $MAPbI_3$ perovskite in a one-step approach. They found that the gradual annealing process favors crystallization of perovskite and facilitates the formation of homogenous surface coverage and micrometer-scale carrier diffusion lengths. Consequently, the PSC device showed a high PCE up to 15% and good reproducibility with no obvious hysteresis (see Fig. 15c). Furthermore, Bolink group[144] investigated the effect of an alternative precursor, lead acetate, on the preparation of planar PSC device. By substituting lead acetate for lead iodide, they obtained smooth perovskite film that are pinhole-free over a large area; the PSC device exhibited a remarkably low hysteresis which is also independent of the scan speed (see Fig. 15d).

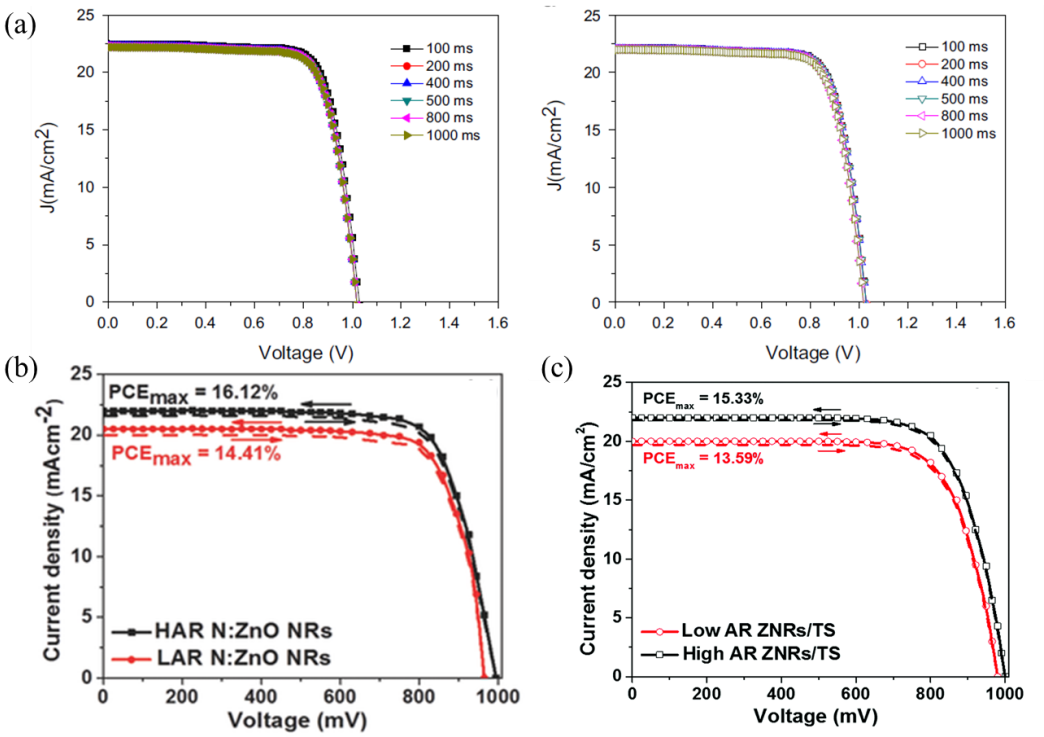

Fig. 16 Hysteresis-free J-V curves measured form different mesoscopic PSC devices: (a) PSC based on Li-treated TiO_2 photoanode measured by forward scan (left) and reverse scan (right). Reprinted with the permission from Ref. [145]; (b) PSC device based on N:ZnO nanorrods. Reprinted with the permission from Ref. [155]; (c) PSC device based on ZnO nanorods/TiO_2 shell (ZNR/TS) heterostructured photoanode. Reprinted with the permission from Ref.[156].

For the mesoscopic PSC device, TiO_2 is typically used as the N-type contact to transport photoelectrons. However, it has been reported that the present paradigm material TiO_2 may not be the best electron-transporting material for $MAPbI_3$-based PSC device, as the electron transfer from perovskite to TiO_2 can be retarded by an interfacial potential barrier.[101] Therefore tailoring the electronic band structure by interface engineering could be helpful. The Im group developed a Li-treated mesoscopic TiO_2 photoanode with lower conduction band edge and better conductivity in comparison with the untreated one.[145] The resulting PSC device showed a superior PCE up to 17.25% and no significant hysteretic effect was observed in its J-V curve (see Fig. 16a). The Ginger group added Zr into the Ti precursor solution (Zr/Ti molar ratio of 5%) in the synthesis of TiO_2 and .[146] This doping increases the carrier lifetime to microsecond range and also the charge densities in the Zr-TiO_2 electrodes. Furthermore, a pyridine treatment has also been used to modify the interface between perovskite and HTM. As a result, these Zr-TiO_2 electrodes and the pyridine treatment give rise to an increase in PCE and a decrease in hysteresis of the PSC devices.

ZnO is another kind of N-type contact in PSC.[121, 147-154] The Amassian group[155] employed ZnO nanorods with different aspect ratios, which were also doped with nitrogen. In this study, it was found that PSC device based on such ZnO rods became nearly hysteresis-free with a high PEC of 16.1% (Fig. 16b). Still ZnO nanorods, Mahmood and Swain[156] demonstrated that a shell TiO_2 shell formed on high aspect ratio ZnO nanorods can reduce the carrier recombination rate in comparison with the bare ZnO. PSC device based on this core-shell structured photoanode demonstrated a maximum PCE up to 15.3% and no significant hysteretic effect can be observed in the J-V curve (Fig. 16c). In addition, C_{60}[157] and CuI[158] have been reported effective in restraining the hysteresis when used as hole-blocking layer and HTM, respectively.

Conclusion

Organometal trihalide perovskites have evolved as low-cost, low-temperature processable, versatile, and multifunctional materials that are being explored as both the effective light absorber and charge transporter in solar cells. The large absorption coefficient and high charge carrier mobility of perovskites brings unique advantages to PSCs over other third-generation solar cells. Currently, high power conversion efficiencies over 20% has been demonstrated in PSC device, which already surpasses that of the amorphous silicon solar cell and is comparable to multicrystalline silicon solar cell. Other advantages of PSCs device cost-effective fabrication using facile techniques such as screen-printing, spin-coating, and

roll-to-roll printing. Despite the fast advance of the efficiency, the pitfalla of perovskite solar cells are also obvious. Before their commercialization in photovoltaic applications, the instability issue of PSCs under outdoor condition must be resolved. Employing HTM as hole-transporter for solid-state PSCs is a critical improvement in stability compared to the early devices based on liquid electrolytes, but still not good enough. Fundamental wise, the exact mechanism of degradation still need more investigation, but it is generally believed that moisture, oxygen and UV light are the major factors to the decomposition of perovskite in ambient air. Although these degradation pathways can be circumvented in certain degree by proper encapsulation of the PSC device (including water-proof and airtight coating and UV-protective coating), the encapsulation also increases the cost. Hence, to maintain the stability of perovskite as well as other parts in PSC devices (electrode materials, HTM and additives) is one technologically viable option. Chemical modification of perovskites, including the halide alteration and design of 2D perovskite, has provided promising results with significantly enhanced stability in humid environment. Generally, the condition for the stability test includes 1000 h in full sunlight at 85% humidity and 85 °C, while for industry photovoltaics application it requires 20 years. Furthermore, an anomalous hysteresis effect is common in the J-V characteristics of PSC devices, resulting in an appreciable difference in the PCEs. Such hysteretic behavior always creates doubts about the device performance, which is being suspected to have been over-estimated. Hence, fabricating PSCs with long-term stability and reliable high efficiency is a systematic and very multi-disciplinary project, and requires contributions from semiconductor physics, organic chemists, material scientists and engineers. All in all, perovskite solar cells are so far still an excitement in research labs; but the future is certainly bright.

Acknowledgments

This work is support by Singapore-Berkeley Research Initiative for Sustainable Energy (SinBeRISE) program, and the Singapore Ministry of Education Academic Research Fund Tier 3 (MOE2011-T3-1-005).

References

[1] B. Parida, S. Iniyan, R. Goic, *Renewable and Sustainable Energy Reviews* **2011**, *15*, 1625.

[2] Y. Xing, P. Han, S. Wang, P. Liang, S. Lou, Y. Zhang, S. Hu, H. Zhu, C. Zhao, Y. Mi, *Renewable and Sustainable Energy Reviews* **2015**, *51*, 1697.

[3] J. Yan, B. R. Saunders, *RSC Adv.* **2014**, *4*, 43286.

[4] G. S. Long, M. Wei, R. D. Willett, *Inorg. Chem.* **1997**, *36*, 3102.

[5] Y. Wu, W.-H. Zhu, S. M. Zakeeruddin, M. Grätzel, *ACS Appl. Mater. Interfaces* **2015**, *7*, 9307.

[6] J. Bisquert, D. Cahen, G. Hodes, S. Rühle, A. Zaban, *J. Phys. Chem. B* **2004**, *108*, 8106.

[7] L. Lu, M. A. Kelly, W. You, L. Yu, *Nat Photon* **2015**, *9*, 491.

[8] G. Li, R. Zhu, Y. Yang, *Nat Photon* **2012**, *6*, 153.

[9] S. Mathew, A. Yella, P. Gao, R. Humphry-Baker, F. E. CurchodBasile, N. Ashari-Astani, I. Tavernelli, U. Rothlisberger, K. NazeeruddinMd, M. Grätzel, *Nature Chemistry* **2014**, *6*, 242.

[10] J. You, L. Dou, K. Yoshimura, T. Kato, K. Ohya, T. Moriarty, K. Emery, C.-C. Chen, J. Gao, G. Li, Y. Yang, *Nat. Commun.* **2013**, *4*, 1446.

[11] Z. Cheng, J. Lin, *CrystEngComm* **2010**, *12*, 2646.

[12] C. A. Randall, A. S. Bhalla, T. R. Shrout, L. E. Cross, *J. Mater. Res.* **1990**, *5*, 829.

[13] D. Weber, *Z. Naturforsch.* **1978**, *33b*, 1443.

[14] J. H. Im, J. Chung, S. J. Kim, N. G. Park, *Nanoscale Res. Lett.* **2012**, *7*, 353.

[15] K. Yamada, K. Isobe, T. Okuda, Y. Furukawa, *Zeitschrift für Naturforschung A* **1994**, *49a*, 258.

[16] K. Futterer, W. Depmeier, V. Petricek, *Acta Crystallogr. Sect. B.* **1995**, *51*, 768.

[17] D. B. Mitzi, K. Liang, *J. Solid State Chem.* **1997**, *134*, 376.

[18] C. C. Stoumpos, C. D. Malliakas, M. G. Kanatzidis, *Inorg. Chem.* **2013**, *52*, 9019.

[19] D. B. Mitzi, *J. Chem. Soc., Dalton Trans.* **2001**, 1.

[20] D. B. Mitzi, C. A. Feild, W. T. A. H. &, A. M. Guloy, *Nature* **1994**, *369*, 467.

[21] S. Wang, D. B. Mitzi, C. A. Feild, A. Guloy, *J. Am. Chem. Soc.* **1995**, *117*, 5297.

[22] G. A. Mousdis, V. Gionis, G. C. Papavassiliou, C. P. Raptopoulou, A. Terzis, *J. Mater. Chem.* **1998**, *8*, 2259.

[23] K. Yamada, Y. Kuranaga, K. Ueda, S. Goto, T. Okuda, Y. Furukawa, *Bull. Chem. Soc. Japan* **1998**, *71*, 127.

[24] D. B. Mitzi, C. A. Feild, Z. Schlesinger, R. B. Laibowitz, *J. Solid State Chem.* **1995**, *114*, 159.

[25] A. Poglitsch, D. Weber, *J. Chem. Phys.* **1987**, *87*, 6373.

[26] O. Knop, R. E. Wasylishen, M. A. White, T. S. Cameron, M. J. M. V. Oort, *Can. J. Chem.* **1990**, *68*, 412.

[27] K. Yamada, *Z. Naturforsch.* **1991**, *46A*, 307.

[28] D. Weber, *Z. Naturforsch.* **1978**, *33B*, 862.

[29] D. B. Mitzi, *J. Mater. Chem.* **2004**, *14*, 2355.

[30] D. B. Mitzi, C. A. Feild, W. T. A. Harrison, A. M. Guloy, *Nature* **1994**, *369*, 467.

[31] D. B. Mitzi, S. Wang, C. A. Feild, C. A. Chess, A. M. Guloy, *Science* **1995**, *267*, 1473.

[32] C. R. Kagan, D. B. Mitzi, C. D. Dimitrakopoulos, *Science* **1999**, *286*, 945.

[33] M. Era, T. Tsutsui, S. Saito, *Appl. Phys.Lett.* **1995**, *67*, 2436.

[34] K. Chondroudis, D. B. Mitzi, *Chem. Mater.* **1999**, *11*, 3028.

[35] A. Kojima, M. Ikegami, K. Teshima, T. Miyasaka, *Chem. Lett.* **2012**, *41*, 397.

[36] D. B. Mitzi, C. D. Dimitrakopoulos, L. L. Kosbar, *Chem. Mater.* **2001**, *13*, 3728.

[37] J. L. Knutson, J. D. Martin, D. B. Mitzi, *Inorg. Chem.* **2005**, *44*, 4699.

[38] D. B. Mitzi, in *Prog. Inorg. Chem.*, John Wiley & Sons, Inc., **2007**, 1.

[39] A. Kojima, K. Teshima, Y. Shirai, T. Miyasaka, *J. Am. Chem. Soc.* **2009**, *131*, 6050.

[40] J. H. Im, C. R. Lee, J. W. Lee, S. W. Park, N. G. Park, *Nanoscale* **2011**, *3*, 4088.

[41] U. Bach, D. Lupo, P. Comte, J. E. Moser, F. Weissortel, J. Salbeck, H. Spreitzer, M. Gratzel, *Nature* **1998**, *395*, 583.

[42] H.-S. Kim, C.-R. Lee, J.-H. Im, K.-B. Lee, T. Moehl, A. Marchioro, S.-J. Moon, R. Humphry-Baker, J.-H. Yum, J. E. Moser, *Sci. Rep.* **2012**, *2*.

[43] M. M. Lee, J. Teuscher, T. Miyasaka, T. N. Murakami, H. J. Snaith, *Science* **2012**, *338*, 643.

[44] H. S. Kim, C. R. Lee, J. H. Im, K. B. Lee, T. Moehl, A. Marchioro, S. J. Moon, R. Humphry-Baker, J. H. Yum, J. E. Moser, M. Gratzel, N. G. Park, *Scientific reports* **2012**, *2*, 591.

[45] L. Etgar, P. Gao, Z. Xue, Q. Peng, A. K. Chandiran, B. Liu, M. K. Nazeeruddin, M. Gratzel, *J. Am. Chem. Soc.* **2012**, *134*, 17396.

[46] F. Huang, Y. Dkhissi, W. Huang, M. Xiao, I. Benesperi, S. Rubanov, Y. Zhu, X. Lin, L. Jiang, Y. Zhou, A. Gray-Weale, J. Etheridge, C. R. McNeill, R. A. Caruso, U. Bach, L. Spiccia, Y.-B. Cheng, *Nano Energy* **2014**.

[47] S. Das, B. Yang, G. Gu, P. C. Joshi, I. N. Ivanov, C. M. Rouleau, T. Aytug, D. B. Geohegan, K. Xiao, *ACS Photonics* **2015**, *2*, 680.

[48] Y. Deng, E. Peng, Y. Shao, Z. Xiao, Q. Dong, J. Huang, *Energy Environ. Sci.* **2015**, *8*, 1544.

[49] B. R. Sutherland, S. Hoogland, M. M. Adachi, P. Kanjanaboos, C. T. Wong, J. J. McDowell, J. Xu, O. Voznyy, Z. Ning, A. J. Houtepen, E. H. Sargent, *Adv Mater* **2014**.

[50] X.-P. Cui, K.-J. Jiang, J.-H. Huang, X.-Q. Zhou, M.-J. Su, S.-G. Li, Q.-Q. Zhang, L.-M. Yang, Y.-L. Song, *Chem. Commun.* **2015**.

[51] C. K. Chen, Y. P. Shen, H. M. Chen, C. J. Chen, T. S. Chan, J. F. Lee, R. S. Liu, *Eur. J. Inorg. Chem.* **2014**, 773.

[52] J. Burschka, N. Pellet, S. J. Moon, R. Humphry-Baker, P. Gao, M. K. Nazeeruddin, M. Gratzel, *Nature* **2013**, *499*, 316.

[53] M. A. Green, K. Emery, Y. Hishikawa, W. Warta, E. D. Dunlop, *Progress in Photovoltaics: Research and Applications* **2015**, *23*, 1.

[54] M. Liu, M. B. Johnston, H. J. Snaith, *Nature* **2013**, *501*, 395.

[55] C. W. Chen, H. W. Kang, S. Y. Hsiao, P. F. Yang, K. M. Chiang, H. W. Lin, *Adv. Mater.* **2014**, *26*, 6647.

[56] Z. Ku, Y. Rong, M. Xu, T. Liu, H. Han, *Sci. Rep.* **2013**, *3*, 3132.

[57] A. Mei, X. Li, L. Liu, Z. Ku, T. Liu, Y. Rong, M. Xu, M. Hu, J. Chen, Y. Yang, M. Gratzel, H. Han, *Science* **2014**, *345*, 295.

[58] N. J. Jeon, J. H. Noh, W. S. Yang, Y. C. Kim, S. Ryu, J. Seo, S. I. Seok, *Nature* **2015**, *517*, 476.

[59] H. Zhou, Q. Chen, G. Li, S. Luo, T.-b. Song, H.-S. Duan, Z. Hong, J. You, Y. Liu, Y. Yang, *Science* **2014**, *345*, 542.

[60] H. J. Snaith, *J. Phys. Chem. Lett.* **2013**, *4*, 3623.

[61] http://www.nrel.gov/ncpv/images/efficiency_chart.jpg

[62] G. Niu, X. Guo, L. Wang, *J. Mater. Chem. A* **2015**, *3*, 8970.

[63] T. Baikie, Y. Fang, J. M. Kadro, M. Schreyer, F. Wei, S. G. Mhaisalkar, M. Graetzel, T. J. White, *J. Mater. Chem. A* **2013**, *1*, 5628.

[64] J. H. Heo, S. H. Im, J. H. Noh, T. N. Mandal, C.-S. Lim, J. A. Chang, Y. H. Lee, H.-j. Kim, A. Sarkar, K. NazeeruddinMd, M. Gratzel, S. I. Seok, *Nat. Photon.* **2013**, *7*, 486.

[65] S. Aharon, A. Dymshits, A. Rotem, L. Etgar, *J. Mater. Chem. A* **2014**, *3*, 9171.

[66] T. Supasai, N. Rujisamphan, K. Ullrich, A. Chemseddine, T. Dittrich, *Appl. Phys.Lett.* **2013**, *103*, 183906.

[67] A. Dualeh, N. Tétreault, T. Moehl, P. Gao, M. K. Nazeeruddin, M. Grätzel, *Adv. Funct. Mater.* **2014**, *24*, 3250.

[68] J. W. Lee, D. J. Seol, A. N. Cho, N. G. Park, *Adv Mater* **2014**.

[69] N. Pellet, P. Gao, G. Gregori, T.-Y. Yang, M. K. Nazeeruddin, J. Maier, M. Grätzel, *Angew. Chem.* **2014**, *126*, 3215.

[70] H. Han, M. Hu, L. Liu, A. Mei, Y. Yang, T. Liu, *J. Mater. Chem. A* **2014**, *2*, 17115.

[71] G. E. Eperon, S. D. Stranks, C. Menelaou, M. B. Johnston, L. M. Herz, H. J. Snaith, *Energy Environ. Sci.* **2014**, *7*, 982.

[72] T. Leijtens, S. D. Stranks, G. E. Eperon, R. Lindblad, E. M. Johansson, I. J. McPherson, H. Rensmo, J. M. Ball, M. M. Lee, H. J. Snaith, *ACS Nano* **2014**, *8*, 7147.

[73] S. Ahmad, P. K. Kanaujia, W. Niu, J. J. Baumberg, G. Vijaya Prakash, *ACS Appl. Mater. Interfaces* **2014**, *6*, 10238.

[74] J. M. Frost, K. T. Butler, F. Brivio, C. H. Hendon, M. van Schilfgaarde, A. Walsh, *Nano Lett.* **2014**, *14*, 2584.

[75] Y. Zhao, K. Zhu, *Chem. Commun.* **2014**, *50*, 1605.

[76] A. Fujishima, T. N. Rao, D. A. Tryk, *J. Photochem. Photobiol. C: Photochem. Rev.* **2000**, *1*, 1.

[77] S. Ito, S. Tanaka, K. Manabe, H. Nishino, *J. Phys. Chem. C* **2014**, *118*, 16995.

[78] S. K. Pathak, A. Abate, T. Leijtens, D. J. Hollman, J. Teuscher, L. Pazos, P. Docampo, U. Steiner, H. J. Snaith, *Adv. Energy Mater.* **2014**, *4*, 1301667.

[79] T. Leijtens, G. E. Eperon, S. Pathak, A. Abate, M. M. Lee, H. J. Snaith, *Nat. Commun.* **2013**, *4*, 2885.

[80] X. Dong, H. Hu, b. lin, J. N. Ding, N. Yuan, *Chem. Commun.* **2014**.

[81] W. Li, H. Dong, L. Wang, N. Li, X. Guo, J. Li, Y. Qiu, *J. Mater. Chem. A* **2014**, *2*, 13587.

[82] J. Krüger, R. Plass, L. Cevey, M. Piccirelli, M. Grätzel, U. Bach, *Appl. Phys.Lett.* **2001**, *79*, 2085.

[83] H. J. Snaith, M. Grätzel, *Appl. Phys.Lett.* **2006**, *89*.

[84] U. B. Cappel, T. Daeneke, U. Bach, *Nano Lett.* **2012**, *12*, 4925.

[85] L. Yang, B. Xu, D. Bi, H. Tian, G. Boschloo, L. Sun, A. Hagfeldt, E. M. J. Johansson, *J. Am. Chem. Soc.* **2013**, *135*, 7378.

[86] Z. Hawash, L. K. Ono, S. R. Raga, M. V. Lee, Y. Qi, *Chem. Mater.* **2015**, *27*, 562.

[87] L. K. Ono, S. R. Raga, M. Remeika, A. J. Winchester, A. Gabe, Y. Qi, *J. Mater. Chem. A* **2015**.

[88] M.-C. Jung, S. R. Raga, L. K. Ono, Y. Qi, *Sci. Rep.* **2015**, *5*, 9863.

[89] A. Dualeh, T. Moehl, N. Tétreault, J. Teuscher, P. Gao, M. K. Nazeeruddin, M. Grätzel, *ACS Nano* **2014**, *8*, 362.

[90] H. J. Snaith, A. Abate, J. M. Ball, G. E. Eperon, T. Leijtens, N. K. Noel, S. D. Stranks, J. T.-W. Wang, K. Wojciechowski, W. Zhang, *J. Phys. Chem. Lett.* **2014**, *5*, 1511.

[91] J. M. Frost, K. T. Butler, A. Walsh, *Apl Materials* **2014**, *2*, 081506.

[92] J. Wei, Y. Zhao, H. Li, G. Li, J. Pan, D. Xu, Q. Zhao, D. Yu, *J. Phys. Chem. Lett.* **2014**, *5*, 3937.

[93] H.-W. Chen, N. Sakai, M. Ikegami, T. Miyasaka, *J. Phys. Chem. Lett.* **2015**, *6*, 164.

[94] Y. Shao, Z. Xiao, C. Bi, Y. Yuan, J. Huang, *Nat Commun* **2014**, *5*, 5784.

[95] W. Li, H. Dong, G. Dong, L. Wang, *Org. Electron.* **2015**, *26*, 208.

[96] C. Eames, J. M. Frost, P. R. Barnes, B. C. O'Regan, A. Walsh, M. S. Islam, *Nat Commun* **2015**, *6*, 7497.

[97] E. J. Juarez-Perez, R. S. Sanchez, L. Badia, G. Garcia-Belmonte, Y. S. Kang, I. Mora-Sero, J. Bisquert, *J. Phys. Chem. Lett.* **2014**, *5*, 2390.

[98] T. Y. Yang, G. Gregori, N. Pellet, M. Gratzel, J. Maier, *Angew Chem Int Ed Engl* **2015**, *54*, 7905.

[99] E. L. Unger, E. T. Hoke, C. D. Bailie, W. H. Nguyen, A. R. Bowring, T. Heumuller, M. G. Christoforo, M. D. McGehee, *Energy Environ. Sci.* **2014**, *7*, 3690.

[100] R. Gottesman, E. Haltzi, L. Gouda, S. Tirosh, Y. Bouhadana, A. Zaban, E. Mosconi, F. De Angelis, *J. Phys. Chem. Lett.* **2014**, *5*, 2662.

[101] B. Wu, K. Fu, N. Yantara, G. Xing, S. Sun, T. C. Sum, N. Mathews, *Adv. Energy Mater.* **2015**, n/a.

[102] Z. Cheng, J. Lin, *CrystEngComm* **2010**, *12*, 2646.

[103] J. H. Noh, S. H. Im, J. H. Heo, T. N. Mandal, S. I. Seok, *Nano Lett.* **2013**, *13*, 1764.

[104] D. B. Mitzi, C. D. Dimitrakopoulos, J. Rosner, D. R. Medeiros, Z. Xu, C. Noyan, *Adv. Mater.* **2002**, *14*, 1772.

[105] E. Mosconi, A. Amat, M. K. Nazeeruddin, M. Grätzel, F. De Angelis, *J. Phys. Chem. C* **2013**, *117*, 13902.

[106] M. M. Lee, J. Teuscher, T. Miyasaka, T. N. Murakami, H. J. Snaith, *Science* **2012**, *338*, 643.

[107] G. C. Papavassiliou, J. Koutselas, D. Lagouvardos, C. CH3NH3PbCl, C. N. P. CH3NH3PbBr, C. N. S. CH3NH3SnBr, *ZEITSCHRIFT FUR NATURFORSCHUNG B* **1993**, *48*, 1013.

[108] I. C. Smith, E. T. Hoke, D. Solis-Ibarra, M. D. McGehee, H. I. Karunadasa, *Angew. Chem. Int. Ed.* **2014**, *53*, 11232.

[109] S. N. Habisreutinger, T. Leijtens, G. E. Eperon, S. D. Stranks, R. J. Nicholas, H. J. Snaith, *Nano Lett.* **2014**.

[110] P. Umari, E. Mosconi, F. De Angelis, *Sci. Rep.* **2014**, *4*, 4467.

[111] L. Zheng, Y. H. Chung, Y. Ma, L. Zhang, L. Xiao, Z. Chen, S. Wang, B. Qu, Q. Gong, *Chem. Commun.* **2014**, *50*, 11196.

[112] M. Zhang, M. Lyu, H. Yu, J. H. Yun, Q. Wang, L. Wang, *Chemistry* **2015**, *21*, 434.

[113] Y. Xiao, G. Han, Y. Chang, H. Zhou, M. Li, Y. Li, *J. Power Sources* **2014**, *267*, 1.

[114] J. Liu, Y. Z. Wu, C. J. Qin, X. D. Yang, T. Yasuda, A. Islam, K. Zhang, W. Q. Peng, W. Chen, L. Y. Han, *Energy Environ. Sci.* **2014**, *7*, 2963.

[115] J. Burschka, N. Pellet, S.-J. Moon, R. Humphry-Baker, P. Gao, M. K. Nazeeruddin, M. Grätzel, *Nature* **2013**, *499*, 316.

[116] K. Wojciechowski, M. Saliba, T. Leijtens, A. Abate, H. J. Snaith, *Energy Environ. Sci.* **2014**, *7*, 1142.

[117] Q. Chen, H. Zhou, Z. Hong, S. Luo, H.-S. Duan, H.-H. Wang, Y. Liu, G. Li, Y. Yang, *J. Am. Chem. Soc.* **2013**, *136*, 622.

[118] J. Qiu, Y. Qiu, K. Yan, M. Zhong, C. Mu, H. Yan, S. Yang, *Nanoscale* **2013**, *5*, 3245.

[119] J. H. Heo, S. H. Im, J. H. Noh, T. N. Mandal, C.-S. Lim, J. A. Chang, Y. H. Lee, H.-j. Kim, A. Sarkar, M. K. Nazeeruddin, *Nat. Photon.* **2013**, *7*, 486.

[120] B. Conings, L. Baeten, C. De Dobbelaere, J. D'Haen, J. Manca, H. G. Boyen, *Adv. Mater.* **2014**, *26*, 2041.

[121] D. Bi, G. Boschloo, S. Schwarzmuller, L. Yang, E. M. Johansson, A. Hagfeldt, *Nanoscale* **2013**, *5*, 11686.

[122] J. A. Christians, R. C. Fung, P. V. Kamat, *J. Am. Chem. Soc.* **2014**, *136*, 758.

[123] M. Law, L. E. Greene, A. Radenovic, T. Kuykendall, J. Liphardt, P. Yang, *J. Phys. Chem. B* **2006**, *110*, 22652.

[124] F. Luo, L. Wang, B. Ma, Y. Qiu, *J. Photochem. Photobiol. A: Chem.* **2008**, *197*, 375.

[125] E. Palomares, J. N. Clifford, S. A. Haque, T. Lutz, J. R. Durrant, *Chem. Commun.* **2002**, 1464.

[126] W. Li, J. Li, L. Wang, G. Niu, R. Gao, Y. Qiu, *J. Mater. Chem. A* **2013**, *1*, 11735.

[127] S.-Y. Liu, J. Sheu, C.-K. Tseng, J.-C. Ye, K. Chang, M. Lee, W. Lai, *J. Electrochem. Soc.* **2010**, *157*, B266.

[128] G. Niu, W. Li, F. Meng, L. Wang, H. Dong, Y. Qiu, *Journal of Materials Chemistry A* **2014**, *2*, 705.

[129] P. Da, M. Cha, L. Sun, Y. Wu, Z.-S. Wang, G. Zheng, *Nano Lett.* **2015**, *15*, 3452.

[130] J. Luo, J.-H. Im, M. T. Mayer, M. Schreier, M. K. Nazeeruddin, N.-G. Park, S. D. Tilley, H. J. Fan, M. Grätzel, *Science* **2014**, *345*, 1593.

[131] S. Aharon, S. Gamliel, B. El Cohen, L. Etgar, *Phys. Chem. Chem. Phys.* **2014**, *16*, 10512.

[132] Y. Rong, Z. Ku, A. Mei, T. Liu, M. Xu, S. Ko, X. Li, H. Han, *J. Phys. Chem. Lett.* **2014**, *5*, 2160.

[133] H. Han, L. Zhang, T. Liu, L. Liu, M. Hu, Y. Yang, A. Mei, *J. Mater. Chem. A* **2015**, *3*, 9165.

[134] Z. Wei, H. Chen, K. Yan, S. Yang, *Angew. Chem. Int. Ed.* **2014**, *53*, 13239.

[135] S. Pang, H. Hu, J. Zhang, S. Lv, Y. Yu, F. Wei, T. Qin, H. Xu, Z. Liu, G. Cui, *Chem. Mater.* **2014**, *26*, 1485.

[136] H. Zhou, Y. Shi, Q. Dong, H. Zhang, Y. Xing, K. Wang, Y. Du, T. Ma, *J. Phys. Chem. Lett.* **2014**, 3241.

[137] X. Xu, Z. Liu, Z. Zuo, M. Zhang, Z. Zhao, Y. Shen, H. Zhou, Q. Chen, Y. Yang, M. Wang, *Nano Lett.* **2015**, *15*, 2402.

[138] H. Wei, J. Xiao, Y. Yang, S. Lv, J. Shi, X. Xu, J. Dong, Y. Luo, D. Li, Q. Meng, *Carbon* **2015**, *93*, 861.

[139] J. Xu, A. Buin, A. H. Ip, W. Li, O. Voznyy, R. Comin, M. Yuan, S. Jeon, Z. Ning, J. J. McDowell, P. Kanjanaboos, J. P. Sun, X. Lan, L. N. Quan, D. H. Kim, I. G. Hill, P. Maksymovych, E. H. Sargent, *Nat Commun* **2015**, *6*, 7081.

[140] J. Xiong, B. Yang, R. Wu, C. Cao, Y. Huang, C. Liu, Z. Hu, H. Huang, Y. Gao, J. Yang, *Org. Electron.* **2015**, *24*, 106.

[141] N. Tripathi, M. Yanagida, Y. Shirai, T. Masuda, L. Han, K. Miyano, *J. Mater. Chem. A* **2015**, *3*, 12081.

[142] C.-G. Wu, C.-H. Chiang, Z.-L. Tseng, M. K. Nazeeruddin, A. Hagfeldt, M. Gratzel, *Energy Environ. Sci.* **2015**.

[143] M.-F. Xu, H. Zhang, S. Zhang, H. L. Zhu, H.-M. Su, J. Liu, K. S. Wong, L.-S. Liao, W. C. H. Choy, *J. Mater. Chem. A* **2015**, *3*, 14424.

[144] D. Forgacs, M. Sessolo, H. J. Bolink, *J. Mater. Chem. A* **2015**, *3*, 14121.

[145] J. H. Heo, M. S. You, M. H. Chang, W. Yin, T. K. Ahn, S.-J. Lee, S.-J. Sung, D. H. Kim, S. H. Im, *Nano Energy* **2015**, *15*, 530.

[146] H. Nagaoka, F. Ma, D. W. deQuilettes, S. M. Vorpahl, M. S. Glaz, A. E. Colbert, M. E. Ziffer, D. S. Ginger, *J Phys Chem Lett* **2015**, *6*, 669.

[147] M. H. Kumar, N. Yantara, S. Dharani, M. Graetzel, S. Mhaisalkar, P. P. Boix, N. Mathews, *Chem Commun (Camb)* **2013**, *49*, 11089.

[148] J. Dong, Y. Zhao, J. Shi, H. Wei, J. Xiao, X. Xu, J. Luo, J. Xu, D. Li, Y. Luo, Q. Meng, *Chem. Commun.* **2014**.

[149] J. Kim, G. Kim, T. K. Kim, S. Kwon, H. Back, J. Lee, S. H. Lee, H. Kang, K. Lee, *J. Mater. Chem. A* **2014**.

[150] L. Loh, J. Briscoe, S. Dunn, *Nanoscale* **2014**, *6*, 7072.

[151] F. J. Ramos, M. C. Lopez-Santos, E. Guillen, M. K. Nazeeruddin, M. Graetzel, A. R. Gonzalez-Elipe, S. Ahmad, *Chemphyschem* **2014**, *15*, 1148.

[152] J. Zhang, P. Barboux, T. Pauporté, *Adv. Energy Mater.* **2014**, *4*, n/a.

[153] S. He, L. Qiu, X. Fang, G. Guan, P. Chen, Z. Zhang, H. Peng, *J. Mater. Chem. A* **2015**.

[154] J. Zhang, E. J. Juarez-Perez, I. Mora Sero, B. Viana, T. Pauporte, *J. Mater. Chem. A* **2015**.

[155] K. Mahmood, B. S. Swain, A. Amassian, *Adv. Energy Mater.* **2015**, n/a.

[156] K. Mahmood, B. S. Swain, A. Amassian, *Nanoscale* **2015**, *7*, 12812.

[157] K. Wojciechowski, T. Leijtens, S. Siprova, C. Schlueter, M. T. Horantner, J. T. Wang, C. Z. Li, A. K. Jen, T. L. Lee, H. J. Snaith, *J Phys Chem Lett* **2015**, *6*, 2399.

[158] G. A. Sepalage, S. Meyer, A. Pascoe, A. D. Scully, F. Huang, U. Bach, Y.-B. Cheng, L. Spiccia, *Adv. Funct. Mater.* **2015**, n/a.